Hexatic undulations in curved geometries

Peter Lenz* and David R. Nelson
Lyman Laboratory of Physics, Harvard University, Cambridge, Massachusetts 02138
(Received 31 October 2002; published 14 March 2003)

We discuss the influence of two-dimensional hexatic order on capillary waves and undulation modes in spherical and cylindrical geometries. In planar geometries, extended bond-orientational order has only a minor effect on the fluctuations of liquid surfaces or lipid bilayers. However, in curved geometries, the long-wavelength spectrum of these ripples is altered. We calculate this frequency shift and discuss applications to spherical vesicles, liquid metal droplets, bubbles and cylindrical jets coated with surface-active molecules, and to multielectron bubbles in liquid helium at low temperatures. Hexatic order also leads to a shift in the threshold for the fission instability of charged droplets and bubbles, and for the Plateau-Rayleigh instability of liquid jets.

DOI: 10.1103/PhysRevE.67.031502 PACS number(s): 64.70.Dv, 68.03.−g, 82.70.−y

I. INTRODUCTION

In two dimensions the melting from a crystal to an isotropic liquid can be a two-stage process [1], driven by the sequential unbinding of dislocations [1,2] and disclinations [1]. At low temperatures $T<T_m$ dislocations are suppressed due to their cost in elastic energy. However, their free energy decreases with increasing temperature. At a temperature $T=T_m$, the quasi-long-ranged translational order of the crystal is destroyed by the dissociation of dislocation pairs. This transition leads to an intervening hexatic phase, which still exhibits extended orientational correlations. The unbinding of disclination pairs sets in at a higher temperature $T=T_i$. In this second transition the quasi-long-ranged orientational order of the hexatic phase is destroyed, leading to an isotropic liquid. This mechanism allows the melting transition to be continuous in contrast to the first-order melting (directly to an isotropic fluid) predicted by Landau [3].

Several experimental systems have illuminated the nature of two-dimensional (2D) melting. A nearly ideal system is electrons on helium [4–6]. The electrons are trapped on the surface of liquid helium by a submerged, positively charged capacitor plate. Their separations are rarely less than 1000 Å, so the in-plane physics is that of classical particles with a repulsive $1/r$ potential. The liquid helium does not freeze at low temperatures, so it is possible to cool the electrons on this liquid substrate well below a sharply defined 2D freezing temperature ($T_m\sim 0.5$ K) [4]. On the theoretical side, important parameters such as the 2D shear modulus and dislocation core energy are easily calculated with this potential [7]. Computer simulations [8] reveal a shear modulus which appears to drop to zero at the melting temperature. Measurements of the shear modulus [6] and specific heat [5] are *consistent* with a continuous dislocation mediated melting transition. However, in these experiments it is difficult to determine experimentally if hexatic order and a disclination unbinding transition are in fact present above T_m.

However, experimental evidence for hexatic order *has* been found in a variety of other systems, including free standing liquid crystal films [9] and Langmuir-Blodgett surfactant monolayers [10]. A hexatic-to-liquid transition has been observed in two-dimensional magnetic bubble arrays [11]. Furthermore, there is strong support for two-stage continuous melting from recent experiments on two-dimensional colloidal crystals [12,13]. In this case, the colloids can be directly imaged by video microscopy, thus allowing a precise test of the theory.

The modest time scales available even on the fastest computers make equilibration in Monte Carlo or molecular dynamics simulations of two-dimensional melting difficult. However, there is now evidence via computer simulations for continuous melting and a narrow sliver of hexatic phase for hard disks [14] and for particles interacting with a repulsive $1/r^{12}$ potential [15]. There are also indications of defect mediated melting transitions for the familiar Lennard-Jones 6-12 pair potential [16].

In the above experiments, order was typically probed via diffraction or by direct measurement of correlation functions in real space. It is difficult to use these methods, however, when hexatic order is present on a curved surface, such as a sphere or a cylinder. Examples where hexatic and crystalline order might be present on a sphere include ''liposomes,'' i.e., closed vesicles composed of lipid bilayers [17,18], the surface of liquid metal droplets confined in Paul traps [19], and multielectron bubbles submerged in liquid helium [20].

Hexatic order in spherical liposomes seems likely because flat two-dimensional planar layers of lipids such as DMPC (dimyristoyl phosphatidylcholine) [21], similar to free standing liquid crystal films [22], can exist in a variety of states with different degrees of positional and orientational order. Examples include fluid, smectic *C*, hexatic and crystalline phases.

Curved hexatic order may also arise on droplets. Celestini *et al.* [23] have found evidence from computer simulations for extended orientational correlations at the flat surface of supercooled heavy noble liquid metals, such as Au, Pt, or Ir. These metals have a general tendency to reduce the interatomic distance at the surface. Upon supercooling this effect is enhanced, leading, generally to a two-dimensional crystalline surface layer. Under suitable cooling conditions, hexatic

*Present address: Institut Curie, UMR 168, 26 rue d'Ulm, F-75248 Paris Cédex 05, France.

order can also appear on the free surface of undercooled liquid metals [23]. Surface hexatic order may also occur on water droplets coated with surface-active molecules, given that there are already extensive observations of this type of order in Langmuir-Blodgett monolayers [10].

Finally, one might expect spherical hexatic and crystalline order in multielectron bubbles in helium. These arise when the helium surface undergoes an electrohydrodynamic instability at high electron densities. The surface then develops a regular array of dimples, each containing 10^6 electrons or more. As the electric field increases these dimples deepen until eventually electrons break through the interface. After subduction, large numbers of electrons (10^5–10^7) then coat the inside wall of a large (10–100 μm radius) sphere of helium vapor. These multielectron bubbles have been observed to move through the helium after their creation above a protruding anode [20,24,25]. They are stable at low electron densities since the Coulomb pressure can be compensated by the surface tension of the helium liquid-vapor interface. However, if the electron density becomes too high the electrostatic repulsion exceeds the balancing force and the bubble undergoes fission [26,27].

One might hope that bond-orientational order in a flat membrane or an interface could be detected by its effects on the dynamics of undulation modes or capillary waves. Unfortunately, hexatic order couples only to the *Gaussian* curvature [28], which vanishes for a simple sine wave deformation of a flat membrane or an interface [cf. Eqs. (27) and (84) below]. The situation is different, however, when these excitations are superimposed on a nontrivial background geometry such as that of a sphere or a cylinder. In a recent short communication [29], we have determined the effect of hexatic order on the undulation modes and capillary wave excitations for the spherical systems described above. The frequency shift is large for liposomes with hexatic order. Observable effects could also occur for liquid metal droplets, surfactant coated water drops, and in multielectron bubbles in helium. In this paper, we describe hexatic dynamics on spherical surfaces in detail and extend the theory to include cylindrical geometries.

Cylindrical geometries could be realized by, e.g., coating a liquid jet with a hexatic monolayer. These jets will (similar to conventional liquids) undergo the well-known Plateau-Rayleigh shape instability as soon as their length reaches a critical size. However, the stiffness associated with extended orientational correlations shifts the threshold of this instability and alters the decay of the cylinder into a chain of droplets. Cylinders provide also an example where hexatic order is perfectly compatible with the underlying geometry: since the Gaussian curvature of the cylinder vanishes, no disclination defects are present in the ground state to complicate the analysis.

The remainder of this paper is organized as follows. First, we analyze the influence of surface hexatic order on spheres by considering liquid droplets (Sec. II). Then, in Sec. III, we apply our analysis to cylindrical geometries. Here, we concentrate on liquid jets and we determine the effect of hexatic order on the Plateau-Rayleigh instability. Next, we compute the shifted instability due to hexatic order in multielectron bubbles (Sec. IV). As a last application, we investigate in Sec. V the influence of hexatic order on the undulations of spherical vesicles. Finally, in Sec. VI, we elaborate in detail on experimental consequences of our work.

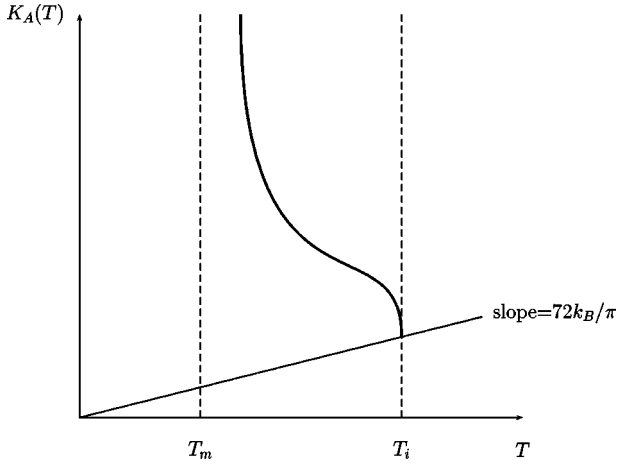

FIG. 1. The hexatic stiffness K_A as function of the temperature T. K_A diverges near T_m and jumps discontinuously to zero at T_i with $\lim_{T\to T_i^-} K_A(T)=72k_BT/\pi$ [1,31].

II. DYNAMICS OF LIQUID DROPLETS WITH HEXATIC ORDER

We first discuss liquid droplets with surface hexatic order. The equilibrium shape minimizes a droplet free energy F_d given by contributions from an interfacial energy and the hexatic degrees of freedom

$$F_d=F_i+F_h\equiv\sigma\int dA+\frac{1}{2}K_A\int dA\, D_in^jD^in_j, \qquad (1)$$

where we use the summation convention throughout and σ denotes the surface tension of the interface of the liquid droplet. For a general manifold with internal coordinates $x=(x^1,x^2)$, the surface element is given by $dA=\sqrt{g(x)}d^2x$, where $g(x)$ is the determinant of the metric tensor $g_{ij}(x)$. For an undeformed sphere with radius R_0, $x\equiv(\theta,\varphi)$ with polar coordinates θ and φ, and $dA=R_0^2\sin\theta d\theta d\varphi$. The quantity $\vec{n}$ is a unit vector in the tangent plane with $n_in^i=1$ which identifies (modulo $2\pi/6$) the long-range correlations in the hexatic bond directions [28]. Here, $D_in^j\equiv g^{jk}D_in_k$, where g^{ij} is the inverse of g_{ij}. The operator D_i denotes a covariant derivative with respect to the metric g_{ij}. Thus, $D_in^j\equiv\partial_in^j+\Gamma^j_{ki}n^k$, where the Γ^j_{ki} are Christoffel symbols of second kind. See, e.g., Ref. [30]. Close to the melting temperature T_m, the hexatic stiffness $K_A\sim E_c(\xi_T/a_0)^2$, where ξ_T is the translational correlation length, a_0 is the particle spacing, and E_c is the dislocation core energy [1]. The ratio K_A/k_BT jumps from an universal value $72/\pi$ to zero when the hexatic melts into an isotropic liquid at $T=T_i^-$ (see Fig. 1) [1].

Droplets have a nearly constant volume V and the corresponding constraint could be included in the free energy F_d. However, here it is easier to first consider shape fluctuations

which explicitly keep the volume fixed. Finally, in Eq. (1) we neglect effects arising from gravity since we only consider droplets with radii $R_0 \ll l_c$ much smaller than the capillary length l_c, which is of order millimeters or more for typical droplets in the earth's gravitational field.

In the following, we will consider the dynamics of shape fluctuations of spherical droplets. As the droplet deforms its geometrical properties change, i.e., the metric and the mean and Gaussian curvature are altered. The free energy (1) thus has a functional dependence on the underlying droplet shape. This dependence can be treated most efficiently by parameterizing the surface of the droplet by its surface vector $\vec{R}$. For a sphere, we have

$$\vec{R}(x^1,x^2) \equiv \vec{R}(\theta,\varphi) = R_0(\theta,\varphi)(\sin\theta\cos\varphi, \sin\theta\sin\varphi, \cos\theta). \tag{2}$$

See Appendix A for important geometrical quantities such as the metric tensor $g_{ij}(x)$, the mean curvature $H(x)$, and the Gaussian curvature $G(x)$ in terms of the surface vector $\vec{R}(x^1,x^2)$.

The fundamental assumption which underlies the hexatic free energy discussed above is that the configuration of minimal elastic energy corresponds to a vector field $\vec{n}_0$, where $\vec{n}_0(x+dx)$ can be obtained from $\vec{n}_0(x)$ by parallel transport of $\vec{n}_0$. On a sphere however, curvature introduces "frustration" since parallel transport of $\vec{n}$ along closed loops on the surface leads to a rotation of $\vec{n}$. Because of this frustration the ground state of hexatic order on a sphere has at least 12 positive disclinations. This constraint is a consequence of the Poincaré index theorem [32], which states that a vector field on a surface with genus g and Euler characteristic $E=2(1-g)$ must have singularities with total vorticity $2\pi E$. As a consequence, order which is identified by a vector order-parameter field on a curved geometry frustrated by a nonzero integrated Gaussian curvature

$$\overline{G} = \int dA G(x) \tag{3}$$

always has topological defects [33]. On a sphere with $g=0$ and $E=2$ hexatics must have a minimum of 12 defects with charges $2\pi/6$ [34].

The energy of an isolated disclination in a hexatic diverges logarithmically in flat space. However, this energy is reduced due to screening by the Gaussian curvature of the sphere. This point can be made more precise by introducing a local bond-angle field θ, the angle between $\vec{n}$ and some local reference frame. The transverse part of θ is then connected with the disclination density [28,33]. As shown in Appendix B, the elastic free energy associated with hexatic order can then be written as [35]

$$F_h = -\frac{1}{2}K_A \int dA \int dA' [G(x)-s(x)]\Gamma(x,x') \times [G(x')-s(x')]. \tag{4}$$

Here, $\Gamma(x,x')$ is the inverse Laplacian on the sphere (see Appendix B), and $s(x)$ the disclination density [33],

$$s(x) \equiv \frac{1}{\sqrt{g(x)}} \sum_{i=1}^{N_d} q_i \delta(x-x_i), \tag{5}$$

with N_d disclinations of charge $q_i = \pm 2\pi/6$ at positions x_i. In deriving Eq. (4), we have assumed that the regular part of the bond-angle field θ^{reg} relaxes rapidly on the time scale of shape deformations. In Sec. V, we will show that this assumption is indeed justified for the systems considered here. Finally, it should be emphasized that Eqs. (4) and (5) hold for arbitrary geometries, not just for that of the sphere (cf. Appendix B).

The defects minimize F_h by arranging themselves to approximately match the Gaussian curvature, which is $G(x) \equiv 1/R_0^2$ for a rigid sphere of radius R_0. Deep in a hexatic phase on a sphere, we expect $N_d=12$, corresponding to 12 fivefold disclinations which lie on the vertices of an icosahedron. With polar coordinates such that there are disclinations at the north and south pole, the 12 defect locations entering Eq. (5) are given by

$$(\theta_k,\varphi_k) \in \left\{ (0,0), \left(\gamma, \frac{2\pi k}{5}\right)_{0\le k\le 4}, \left(\pi-\gamma, \frac{\pi}{5}+\frac{2\pi k}{5}\right)_{0\le k\le 4}, (\pi,0) \right\}, \tag{6}$$

where

$$\gamma \equiv \cos^{-1}\frac{1}{\sqrt{5}}. \tag{7}$$

A. Fluctuation spectrum

To investigate the influence of hexatic order on spherical droplets, we study deformations about the equilibrium configuration. We expand the free energy F_d in a small time-dependent displacement field $\delta\vec{R}(x,t)$, where

$$\vec{R}'(x,t) = \vec{R}_0(x) + \delta\vec{R}(x,t) \tag{8}$$

is the deformed surface and $\vec{R}_0(x)$ is given by Eq. (2). For liquid droplets with hexatic order it is sufficient to consider purely normal displacement fields, cf. Fig. 2. Thus,

$$\delta\vec{R}(x,t) = R_0 \zeta(x,t)\vec{N}(x), \tag{9}$$

where $\vec{N}(x) = \vec{R}_0/R_0$ is the normal vector of the sphere. The dimensionless function ζ can be expanded in terms of spherical harmonics

$$\zeta(x,t) = \sum_{l=0}^{\infty} \sum_{m=-l}^{l} r_{lm}(t) Y_{lm}(x). \tag{10}$$

In the absence of defects, the expansion of F_d in ζ would be straightforward. On the sphere, however, one has to deal with 12 discrete disclination charges which produce a small

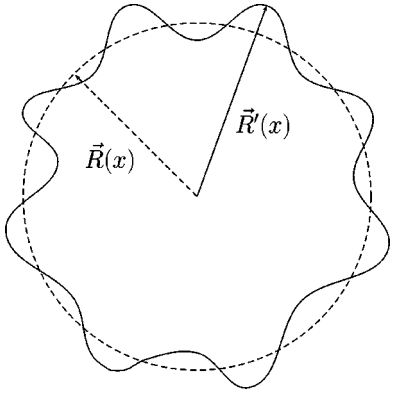

FIG. 2. Parametrization of the droplet shape by the surface vector $\vec{R}$. The deformed surface can be parametrized by $\vec{R}'(x,t) = R_0[1+\zeta(x,t)]\vec{N}$, where $\vec{N}$ is the unit normal.

static icosahedral surface deformation. We initially neglect this discreteness and approximate these defects by a smeared distribution of defect ''charge.'' As will be shown in Sec. II B, corrections arising from the discrete nature of $s(x)$ are irrelevant for the oscillation frequencies $\omega(l)$ with $l<6$. These considerations can be made more precise by expanding $s(x)$ in terms of spherical harmonics

$$s(x) = G_0 + \frac{1}{R_0^2}\sum_{l=1}^{\infty}\sum_{m=-l}^{l} s_{lm} Y_{lm}(x), \tag{11}$$

where G_0 is the undeformed Gaussian curvature, $G_0 = 1/R_0^2$, and $s_{lm} \equiv \Sigma_{i=1}^{12} q_i Y_{lm}^*(x_i)$. To obtain the last equation, we have used the representation of the δ function in terms of spherical harmonics,

$$\delta(\cos\theta - \cos\theta')\,\delta(\varphi-\varphi') = \sum_{l=0}^{\infty}\sum_{m=-l}^{l} Y_{lm}^*(\theta',\varphi') Y_{lm}(\theta,\varphi). \tag{12}$$

In Eq. (4), we initially smear out the disclination charge by setting $s_{lm} \simeq 0$ for all $l>0$.

With this approximation, the hexatic order has no influence on the droplet shape and the equilibrium configuration is a sphere with a radius R_0. However, the presence of hexatic order with a nonzero stiffness constant K_A, nevertheless, has an important effect on the fluctuation spectrum $\omega(l)$ of a spherical droplet.

To calculate $\omega(l)$, we adopt the treatment of capillary waves on spherical droplets without hexatic order [36] and consider the incompressible Navier-Stokes equation for the fluid of the droplet

$$\rho_l \frac{\partial \vec{v}}{\partial t} + \rho_l(\vec{v}\cdot\vec{\nabla})\vec{v} = -\vec{\nabla}p + \eta\nabla^2\vec{v}, \tag{13a}$$

$$\vec{\nabla}\cdot\vec{v} = 0. \tag{13b}$$

Here, p is the hydrostatic pressure in the presence of an interface and ρ_l, η, and $\vec{v}$ denote the density, shear viscosity, and the velocity of the liquid inside the droplet, respectively.

For droplets the inertial terms in the Navier-Stokes equation (13a) dominate and effects of viscosity are irrelevant. Upon neglecting the nonlinear term, the boundary conditions can be treated most efficiently by introducing a velocity potential Φ with $\vec{v} = \vec{\nabla}\Phi$. Then, integration across the droplet interface leads to

$$\rho_l \left.\frac{\partial\Phi(r)}{\partial t}\right|_{r=(R_0+\zeta R_0)^-} - \rho_v \left.\frac{\partial\Phi(r)}{\partial t}\right|_{r=(R_0+\zeta R_0)^+} = \Delta p(x), \tag{14}$$

where ρ_v is the vapor density of the surrounding medium. Equation (14) relates the pressure difference between the inside and outside of the droplet to the generalized pressure discontinuity $\Delta p(x)$ caused by the shape displacement. Since $\vec{\nabla}\cdot\vec{v} = 0$ one has $\nabla^2\Phi = 0$, a Laplace equation with solutions of the form [36]

$$\Phi(r,x,t) = \begin{cases} \sum_{l,m} A_{lm}^{<}(t) Y_{lm}(x)\left(\frac{r}{R_0}\right)^l & \text{for} \quad r<R_0(1+\zeta) \\ \sum_{l,m} A_{lm}^{>}(t) Y_{lm}(x)\left(\frac{R_0}{r}\right)^{l+1} & \text{for} \quad r>R_0(1+\zeta). \end{cases} \tag{15}$$

The displacement field ζ and the velocity potential Φ are related by the boundary condition that the interface velocity must match the fluid velocity,

$$R_0\dot{\zeta} \equiv R_0\frac{\partial\zeta}{\partial t} = \left.\frac{\partial\Phi}{\partial r}\right|_{r=R_0+\zeta R_0}. \tag{16}$$

Hence, the coefficients in Eq. (15) are given by

$$A_{lm}^{>}(t) = -R_0^2\frac{\dot{r}_{lm}(t)}{l+1} \tag{17}$$

and

$$A_{lm}^{<}(t) = R_0^2\frac{\dot{r}_{lm}(t)}{l}. \tag{18}$$

Upon setting

$$\Delta p(x) \equiv \sum_{l,m}\Delta p_{lm}(t) Y_{lm}(x) \equiv -\sum_{l,m}\frac{\delta F_d'(r_{lm})}{R_0^3\,\delta r_{lm}^*} Y_{lm}(x) \tag{19}$$

(where r_{lm}^* denotes the complex conjugate of r_{lm} and F_d' the free energy of the deformed droplet), one then finds

$$\Delta p_{lm}(t)=\left(\frac{\rho_l}{l}+\frac{\rho_v}{l+1}\right)R_0^2\ddot{r}_{lm}(t). \tag{20}$$

Note the influence of hexatic order appears through the term $\delta F_d'/\delta r_{lm}^*$ in Eq. (19).

To determine the coefficients p_{lm} in Eq. (19), one has to calculate the variation of the droplet free energy. Details about this calculation can be found in Appendix C. For small deviations from a spherical shape, the deformed droplet has volume V' with

$$V'-V=R_0^3\left(\sqrt{4\pi}r_{00}+\sum_{l=1}^{\infty}\sum_{m=-l}^{l}|r_{lm}|^2\right)+O(r_{lm}^3) \tag{21}$$

[see Eq. (C6)]. Thus, the volume constraint $V=V'$ appropriate to droplets can be incorporated directly by considering only displacements which fulfill (to leading order in the r_{lm}'s)

$$r_{00}=-\frac{1}{\sqrt{4\pi}}\sum_{l=1}^{\infty}\sum_{m=-l}^{l}|r_{lm}|^2. \tag{22}$$

With the constraint of fixed volume, the interfacial contribution to the free energy becomes

$$\begin{aligned}F_i'&=\sigma\int d^2x\sqrt{g+\delta g}\\&=F_i+\frac{1}{2}\sigma R_0^2\sum_{l=1}^{\infty}\sum_{m=-l}^{l}|r_{lm}|^2(l-1)(l+2),\end{aligned} \tag{23}$$

where $F_i=\sigma 4\pi R_0^2$ is the interfacial free energy of the undeformed droplet. Equation (23) follows from Eqs. (C5) and (22). The hexatic free energy is given by

$$F_h'=\frac{1}{2}K_A\sum_{l=1}^{\infty}\sum_{m=-l}^{l}|r_{lm}|^2\frac{(l-1)^2(l+2)^2}{l(l+1)}, \tag{24}$$

cf. Eq. (C23).

Upon setting $F_d'=F_i'+F_h'$ and

$$r_{lm}=r_{lm}^0(t)e^{-i\omega(l)t}, \tag{25}$$

and evaluating Eq. (19), we find for the fluctuation spectrum (provided $l>0$ and $\rho_v\ll\rho_l$) [37]

$$\omega^2=\frac{\sigma}{\rho_l R_0^3}l(l-1)(l+2)\left[1+\frac{K_A}{\sigma R_0^2}\frac{(l-1)(l+2)}{l(l+1)}\right]. \tag{26}$$

Equation (26) shows that hexatic order only affects undulation modes in a curved geometry: In the flat space limit of large R_0 and $l\gg 1$ with $k\equiv l/R_0$ fixed, one has

$$\omega^2\simeq\frac{k^3}{\rho_l}\left[\sigma+\frac{K_A}{R_0^2}\right], \tag{27}$$

which exhibits explicitely a hexatic correction to the usual capillary wave spectrum. The hexatic contribution, however, drops out as $R_0\to\infty$ and we recover the result for capillary waves of a flat fluid surface [36]. Thus, it is essential to study deformations of a curved geometry to reveal the presence of hexatic order.

In general, the undulation frequency Eq. (26) depends on the ratio $K_A/\sigma R_0^2$, which for hexatic order on surfactant-coated water drops or at the surface of supercooled liquid metal droplets is $K_A/\sigma R_0^2\simeq(\xi_T/R_0)^2(E_c/\sigma a_0^2)$. This ratio grows to become of order $E_c/\sigma a_0^2\simeq O(1)$ close to a continuous hexatic-to-crystal transition, i.e., when $\xi_T\approx R_0$ (see also Sec. VI).

B. Effect of defects on the spectrum

We now take the deformations associated with a discrete array of 12 disclination defects into account, i.e., we consider nonzero s_{lm} with $l>0$ in Eq. (11). We first neglect the possibility of disclination motion. Thus, we assume that on the time scale of the characteristic frequency (26), the disclinations remain in fixed positions which minimize the hexatic free energy of the undeformed sphere. Thus, for $N_d=12$ disclinations at the vertices of an icosahedron, the positions x_i in Eq. (5) are given by Eq. (6). As the sphere is deformed, the hexatic free energy then changes as (up to first order in r_{lm})

$$\delta^{(1)}F_h=-K_A\sum_{l=1}^{\infty}\sum_{m=-l}^{l}\frac{(l-1)(l+2)}{l(l+1)}s_{lm}r_{lm}^*. \tag{28}$$

This follows from Eq. (C23) since δs_{lm} is of order r_{lm} and the terms of order $s_{lm}\delta s_{lm}$ vanish since the defect arrangement on the sphere minimizes F_h. To calculate the variation of the interfacial contribution the volume constraint has to be included in the free energy. Thus, by considering the modified free energy

$$\tilde{F}_d=F_d+\int dVp(x) \tag{29}$$

(where $p\equiv p_{ex}-p_{in}$ is the pressure difference between outside and inside of the droplet), the complete first variation becomes

$$\begin{aligned}\delta^{(1)}\tilde{F}_d=&\sigma\int d^2x\sqrt{g(x)}\,\delta^{(1)}g(x)+\int d^2x\sqrt{g(x)}p\,\delta^{(1)}V(x)\\&-K_A\int d^2x\sqrt{g(x)}\frac{1}{R_0^2}\sum_{l=1}^{\infty}\sum_{m=-l}^{l}\frac{(l-1)(l+2)}{l(l+1)}\\&\times s_{lm}\mathrm{Y}_{lm}(x)\sum_{l',m'}r_{l'm'}^*\mathrm{Y}_{l'm'}^*(x),\end{aligned} \tag{30}$$

where $\delta^{(1)}g$ is given by Eq. (C4) and $\delta^{(1)}V$ by Eq. (C6). The shape equation for quasispherical droplets with hexatic order becomes

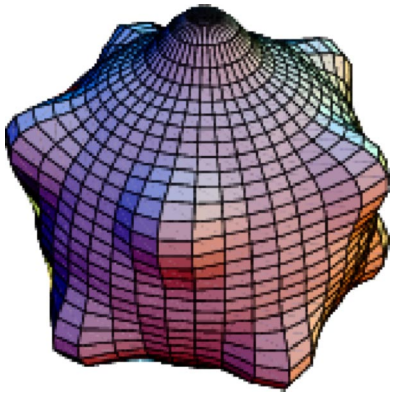

FIG. 3. Shape of a liquid droplet with hexatic order and 12 disclinations lying on the vertices of an icosahedron (surface deformations associated with the defects are exaggerated).

$$p+2\sigma H(x)=K_A\frac{1}{R_0^3}\sum_{l=1}^{\infty}\sum_{m=-l}^{l}\frac{(l-1)(l+2)}{l(l+1)}\mathrm{Y}_{lm}(x)s_{lm}. \tag{31}$$

Thus, nonzero coefficients s_{lm} affect the mean curvature $H(x)$ of the stationary droplet. This equation simplifies upon making the ansatz

$$H(x)=H_0+\widetilde{\delta H}(x)\equiv H_0+\sum_{l=1}^{\infty}\sum_{m=-l}^{l}h_{lm}\mathrm{Y}_{lm}(x), \tag{32}$$

with

$$2H_0\sigma+p=0. \tag{33}$$

One then finds the extremal equation for the mean curvature, namely,

$$2H(x)=2H_0+\frac{K_A}{\sigma R_0^2}\frac{1}{R_0}\sum_{l=1}^{\infty}\sum_{m=-l}^{l}\frac{(l-1)(l+2)}{l(l+1)}s_{lm}\mathrm{Y}_{lm}(x). \tag{34}$$

On the other hand, a deformed sphere has mean curvature [see Eq. (C15)]

$$2H'(x)=\frac{2}{R_0}+\frac{1}{R_0}\sum_{l,m}(l-1)(l+2)r_{lm}\mathrm{Y}_{lm}(x). \tag{35}$$

Comparison of the last two equations then leads immediately to the static surface deformation coefficients

$$r_{lm}^0=s_{lm}\frac{K_A}{\sigma R_0^2 l(l+1)}, \tag{36}$$

for $l>0$ and $r_{lm}^0=0$ for $l=m=0$ in the ground state. Thus, for $K_A\neq 0$ the defects deform the droplet as indicated in Fig. 3. However, nonzero s_{lm} have no influence on the frequencies $\omega(l)$ for $0<l<6$. Indeed, icosahedral symmetry insures that $s_{lm}=0$, and hence $r_{lm}^0=0$, unless $l=6,10,12,\ldots$ [38], so corrections of order s_{lm} have no influence on the frequencies $\omega(l)$ for small l. Thus, provided the positions of the disclinations remain fixed on the time scale of an undulation [i.e., $\delta s_{lm}=0$ holds in Eq. (C23)] the dispersion relation (26) remains valid for $0<l<6$. Because disclination motion is catalyzed by absorption and emission of dislocations with mean spacing ξ_T, the disclination diffusion constant is $D_5\approx(a_0/\xi_T)^2D_0$, where the D_0 is the particle diffusion constant. For a surfactant coated water droplet of radius $R_0=1$ mm one has (for $\sigma=10^{-3}$ N/m) $\omega(l=2)\simeq 100$ Hz and $D_0\simeq 10^{-8}$ cm^2/s. The estimate $(a_0/\xi_T)^2\simeq 10^{-2}$ suggests only minor disclination motion during an undulation period and the spectrum is unaffected for $0<l<6$.

III. DYNAMICS AND INSTABILITIES IN CYLINDRICAL GEOMETRIES

Next, we will discuss the influence of hexatic order on the Plateau-Rayleigh instability [39,40] of cylindrical liquid jets coated with a hexatic monolayer. Because the Gaussian curvature of a cylinder is zero, defect-free hexatic order is perfectly compatible with this geometry in the absence of deformations. However, the hexatic stiffness constant will resist deformations leading to a nonzero Gaussian curvature. The complication of defects in the ground state is absent for hexatic order on cylinders.

The surface vector of a cylinder of undeformed radius R_0 is given by

$$\vec{R}(x)=(R_0\cos\varphi,R_0\sin\varphi,z), \tag{37}$$

with $x=(\varphi,z)$. See again Appendix A for the fundamental geometrical quantities of the cylinder in terms of $\vec{R}$.

The free energy of liquid cylinders (jets) is given by Eq. (1), where now $dA=R_0d\varphi dz$. The displacement field can again be chosen to be purely normal, i.e.,

$$\vec{R}'=\vec{R}+R_0\zeta\vec{N}, \tag{38}$$

where now $\vec{N}(\varphi,z)=(\cos\varphi,\sin\varphi,0)$. The displacement field can be expanded in plane waves

$$\zeta(\varphi,z,t)=\sum_{k,m}r_{km}(t)e^{ikz}e^{im\varphi}, \tag{39}$$

where $k=2\pi n/L$, with $n=0,\pm 1,\pm 2,\ldots$ for a cylinder with length L (we assume periodic boundary conditions along the axis of the cylinder for simplicity) and

$$\sum_{k,m}\equiv\sum_{n=-\infty}^{\infty}\sum_{m=-\infty}^{\infty}. \tag{40}$$

We neglect the density outside the jet ($\rho_v\ll\rho_l$), and make an ansatz for the velocity potential inside in terms of cylindrical coordinates (r,φ,z),

$$\Phi(r,z,\varphi,t)=\sum_{k,m}A_{km}^{<}(t)e^{ikz}e^{im\varphi}I_m(kr), \tag{41}$$

where $I_m(kr)$ is the Bessel function of the first kind of imaginary argument [41]. Equations (14) and (16) remain valid and yield

$$A_{km}^{<}(t)=R_0\frac{\dot{r}_{km}(t)}{kI_m'(kR_0)}, \tag{42}$$

where $I_m'(x)\equiv dI_m(x)/dx$.

If the cylinder is deformed, its surface area and volume change. Equation (C4) of Appendix C implies

$$A'-A=2\pi R_0 L\left[r_{00}+\frac{1}{2}\sum_{k,m}{}'\ (R_0^2k^2+m^2)|r_{km}|^2\right], \tag{43}$$

and with Eq. (C6) one has

$$V'-V=2\pi R_0^2 L\left(r_{00}+\frac{1}{2}\sum_{k,m}{}'\ |r_{km}|^2\right), \tag{44}$$

where the $k=0$, $m=0$ term is excluded from the sum $\Sigma_{k,m}'$.

Upon choosing

$$r_{00}=-\frac{1}{2}\sum_{k,m}{}'\ |r_{km}|^2, \tag{45}$$

the displacement field keeps the volume fixed (corresponding to an incompressible liquid jet) and the difference in interfacial free energy between deformed and undeformed cylinder becomes

$$F_i'-F_i=\pi R_0 L\sigma\sum_{k,m}{}'\ (R_0^2k^2+m^2-1)|r_{km}|^2. \tag{46}$$

Note that this energy difference vanishes for $k=0$, $m=\pm 1$ deformations, corresponding to a uniform sideways translation.

We next calculate the hexatic contribution to the free energy of the deformed cylinder. Equation (C13) with background Gaussian curvature $G=0$ leads to the Gaussian curvature of the deformed state, namely,

$$G'(\varphi,z)=\sum_{k,m}\ k^2 r_{km}e^{ikz}e^{im\varphi}. \tag{47}$$

Equation (4), together with the representation of the Green's function of the Laplacian on the cylinder,

$$\Gamma(x,x')=-\frac{R_0}{2\pi L}\sum_{k,m}{}'\ \frac{e^{ikz}e^{im\varphi}e^{-ikz'}e^{-im\varphi'}}{k^2R_0^2+m^2}, \tag{48}$$

then yields for the hexatic free energy of the deformed cylinder

$$F_h'=\frac{\pi L}{R_0}K_A\sum_{k,m}\ |r_{km}|^2\frac{k^4R_0^4}{k^2R_0^2+m^2}. \tag{49}$$

Equation (14) now leads to

$$\rho_l R_0\ddot{r}_{km}(t)\frac{I_m(kR_0)}{kI_m'(kR_0)}=p_{km}=-\frac{\delta F_d'\{r_{km}\}}{2\pi R_0^2 L\,\delta r_{km}^*}, \tag{50}$$

where

$$\Delta p(z,\varphi)=\sum_{k,m}\ p_{km}e^{ikz}e^{im\varphi}. \tag{51}$$

Upon setting $r_{km}=r_{km}^0e^{-i\omega(k,m)t}$ one finds the fluctuation spectrum of a liquid cylinder with surface hexatic order, namely,

$$\omega^2(k,m)=\frac{\sigma}{\rho_l R_0^3}\frac{I_m'(kR_0)}{I_m(kR_0)}R_0k \times\left[R_0^2k^2+m^2-1+\frac{K_A}{\sigma R_0^2}\frac{k^4R_0^4}{k^2R_0^2+m^2}\right]. \tag{52}$$

When $K_A=0$, Eq. (52) shows $\omega^2<0$ for $m=0$ and $R_0^2k^2<1$. The cylinder thus becomes unstable if $L>2\pi R_0$, leading to the well-known Plateau-Rayleigh instability [39,40]. However, for $K_A\neq 0$ the stability of liquid cylinders is enhanced by hexatic order. The ''fastest growing'' mode k_f, which maximizes $(-\omega^2)$, is now given by

$$\left.\frac{d}{dx}\right|_{x=R_0k}\frac{I_m'(x)}{I_m(x)}x\left(1-x^2-\frac{K_A}{\sigma R_0^2}x^2\right)=0, \tag{53}$$

where $x=kR_0$. Thus, close to the hexatic-to-liquid transition where $K_A/\sigma R_0^2\simeq 1$, one has $R_0^2k_f^2\simeq 0.25$ compared with $R_0^2k_f^2\simeq 0.48$ for $K_A=0$. Thus, the characteristic wavelength $\lambda_f=2\pi/k_f$ of the undulations of the unstable cylinder is significantly stretched by the presence of hexatic order. As we shall see in the following section, hexatic order has a similar effect in stabilizing multielectron bubbles against fission.

IV. HEXATIC DYNAMICS AND FISSION IN MULTIELECTRON BUBBLES

Next, we will discuss multielectron bubbles in liquid ^{4}He. These bubbles can undergo both a freezing transition and a shape instability. Hexatic order affects both the fluctuation spectrum and the instability threshold for fission. The free energy of a multielectron bubble $F_b=F_d+F_c$ is that of a droplet [cf. Eq. (1)] with an additional Coulomb contribution, i.e.,

$$F_b=\sigma\int dA+\frac{1}{2}K_A\int dA\,D_in^jD^in_j + \frac{1}{2\varepsilon}\int dA\int dA'\frac{\rho(x)\rho(x')}{|x-x'|}. \tag{54}$$

Here, $\rho(x)$ denotes the charge distribution on the surface and ε is the dielectric constant of liquid ^{4}He [42]. In an equilibrium fluid, $\rho=eN/4\pi R_0^2$ for a sphere with N electrons.

The assumptions underlying this theoretical description are the following.

(i) The electrons are restricted to the two-dimensional manifold given by the liquid-vapor interface. This is justified since density functional calculations (cf., e.g., Refs. [43,26]) show that the electrons form a thin layer of thickness $\delta \ll R_0$ on the surface with $\delta \simeq 1-4$ nm.

(ii) One can neglect the effects on the shape of the charged bubbles arising from (a) applied electric fields which trap or hold the electrons; (b) the movement of the bubbles in the system; and (c) gravity. Assumption (a) is justified since typical external electric fields are of the order $E \simeq 3$ kV/cm [25], while a charged sphere with radius $R_0 \simeq 10$ μm and $N \simeq 10^7$ produces an electric field ≈ 300 times larger, $E_{sph} = (eN/2R_0^2) \simeq 1$ MV/cm. Similar arguments apply to (b) since typical drag forces are much weaker than the Coulomb forces. Assumption (c) is justified since R_0 is much smaller than the capillary length l_c of liquid helium, $l_c \equiv \sqrt{2\sigma/\rho_l g} \simeq 0.6$ mm.

(iii) We assume that the electrons can be treated classically, i.e., corrections arising from quantum mechanics can be ignored. For electrons on charged bubbles this is justified since at the melting temperature quantum mechanical corrections become only relevant at higher densities, $n \gtrsim 10^{12}$ cm^{-2} [25].

Upon once again neglecting defects by setting $s_{lm} \equiv 0$, $l > 0$, the stationary solutions of the free energy (54) are spherical bubbles. To determine the equilibrium radius we use the partition function of a noninteracting ideal gas to describe the vapor phase. The free energy of a spherical bubble is then given by

$$F(V,T) = \min_R \left\{ k_B T N_{He} \left(\ln \frac{N_{He} \lambda_T^3}{4\pi R^3/3} - 1 \right) + p_{ex} \frac{4\pi}{3} R^3 + 4\pi\sigma R^2 + \frac{N^2 e^2}{2R\varepsilon} \right\}, \tag{55}$$

where N_{He} is the number of helium atoms, λ_T the thermal wavelength, and p_{ex} the pressure outside of the bubble. Minimization with respect to the first term only yields, of course, ideal gas behavior, i.e.,

$$p_{in} V = N_{He} k_B T, \tag{56}$$

where p_{in} is the pressure inside the bubble. However, by taking all contributions into account the equilibrium radius R_0 of a charged multielectron bubble is determined by the Laplace equation

$$p_{in} - p_{ex} = 2\frac{\sigma}{R_0} - \frac{(eN)^2}{8\pi R_0^4 \varepsilon}. \tag{57}$$

Thus, one obtains (for $p_{in} \approx p_{ex}$) as typical length scale for R_0 the classical Coulomb radius

$$R_{cl}^3 = \frac{(eN)^2}{16\pi\sigma\varepsilon}. \tag{58}$$

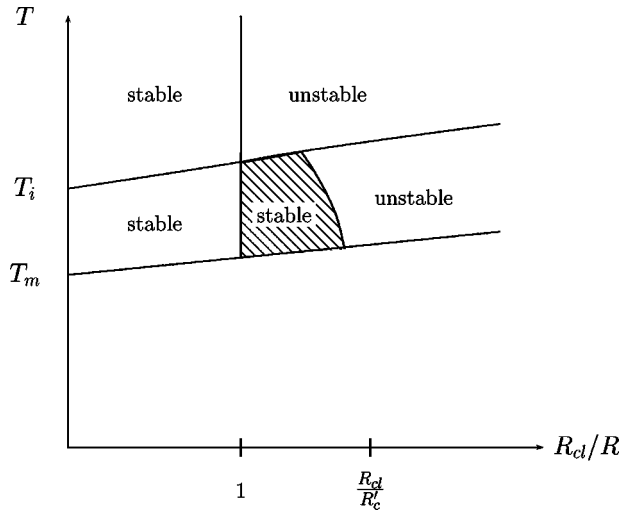

FIG. 4. Schematic stability diagram for multielectron bubbles with hexatic order. The stability of a spherical bubble with radius R and charge eN depends on the temperature T. For hexatics in the temperature range $T_m \lesssim T \lesssim T_i$, bubbles with radii $R_{cl} < R < R_c'$ are stable, whereas for $T \gtrsim T_i$ they are not. The enhanced stability is due to internal hexatic order. We expect an even larger region of enhanced stability for droplets with crystalline order [45].

Within the approximations described above, the fluctuation spectrum of a multielectron bubble with hexatic order can be calculated. Compared with the discussion of Sec. II the only difference arises from the Coulomb contribution. As derived in Appendix C 3 one has for $\rho_v \ll \rho_l$ (thus, neglecting the density inside the bubble)

$$\Delta p_{lm} = \frac{(eN)^2}{4\pi R_0^4 \varepsilon} (l-1) r_{lm}. \tag{59}$$

By combining the last equation with Eqs. (20), (23), and (24) one now finds (for $l > 0$) [44]

$$\omega^2 = \frac{\sigma}{\rho_l R_0^3} (l-1)(l+1) \times \left[(l+2) - 4\frac{R_{cl}^3}{R_0^3} + \frac{K_A}{\sigma R_0^2} \frac{(l-1)(l+2)^2}{l(l+1)} \right]. \tag{60}$$

For $K_A = 0$ spherical bubbles become unstable to fission if $R_0 < R_{cl}$, i.e., $\omega^2(l = l_c) < 0$ for $R_0 < R_{cl}$ and $l_c = 2$ [26,27].

For $K_A \neq 0$ the stability of charged bubbles is *enhanced* by the hexatic order of the electrons on the sphere. Thus, for $T_m < T < T_i$ the unstable mode is still $l_c = 2$, but now $\omega^2(l_c = 2) < 0$ for $R_0 < R_c'$ with $R_c' < R_{cl}$, cf. Fig. 4. The icosahedral symmetry of the deformed shape with $s_{lm} \neq 0$ is too high to have an influence on the fission instability which occurs at $l = 2$, justifying our neglect of disclination defects.

Because the electrons (which determine K_A) are far apart relative to the helium atoms (which determine σ) $K_A/\sigma R_{cl}^2$ will be smaller than for droplets of supercooled liquid metals when $R_0 \simeq R_{cl}$. For helium bubbles with $N \simeq 10^6$ one has $R_{cl} \simeq 10$ μm and we expect (see Sec. VI) that $(K_A/\sigma R_{cl}^2)$

$\simeq 10^{-4}$. *Charged* metal droplets also undergo the same fission instability. Thus, it might be possible to detect the onset of hexatic order by investigating the stability of charged liquid droplets in Paul traps [19].

In the flat space limit ($l \to \infty$, $k = l/R_0$ fixed) one obtains, with $n = eN/4\pi R_0^2$,

$$\rho_{ex}\omega^2(k) = \sigma k^3 - 4\pi k^2 \frac{n^2}{\varepsilon}, \tag{61}$$

in agreement with Ref. [25]. As Eq. (61) shows, planar He interfaces are unstable to deformations with $k < k_c = 4\pi n^2/\sigma\varepsilon$. This is the ''dimple'' instability discussed in the Introduction which triggers the initial creation of multielectron bubbles.

V. DYNAMICS IN HEXATIC MEMBRANES WITH A SPHERICAL TOPOLOGY

As a last application, we discuss the influence of hexatic order on the fluctuations of a spherical vesicle. The free energy F of a hexatic membrane is given by [17,28]

$$F = F_b + F_g + F_h \equiv \frac{1}{2}\kappa \int dA (2H)^2 + \kappa_G \int dA\, G + \frac{1}{2} K_A \int dA\, D_i n^j D^i n_j, \tag{62}$$

where we have neglected spontaneous curvature, and κ and κ_G are the mean and Gaussian rigidity, respectively.

The equilibrium shape of enclosed vesicles (provided fluids inside and outside cannot equilibrate on experimental times scales) often corresponds to the minimum of the free energy (62) with prescribed surface area A and volume V [46] (see also Ref. [47]). The area and volume constraints can be implemented by considering the modified free energy

$$\tilde{F} = F + F_a + F_{vol} \equiv F + \int dA \sigma(x) + \int dV p(x). \tag{63}$$

Often, a constant pressure difference between outside and inside $p \equiv p_{ex} - p_{in} \equiv p^> - p^<$ and surface tension σ are taken as Lagrange multipliers to enforce these constraints. Here, we allow for both spatially varying surface tension $\sigma(x)$ and pressure $p(x)$ to enforce local incompressibility [cf. Eq. (72) below]. In many situations, the average values of σ and p will depend on the volume captured by a vesicle of a given area at the moment of its formation.

In the following analysis, we only consider surface shapes which are topologically equivalent to a sphere. Then, the second term of Eq. (62) can be neglected, since it is a topological invariant. We again temporarily ignore discrete disclination defects and show later that their inclusion does not affect characteristic frequencies $\omega(l)$ with $l < 6$.

Because κ plays a similar role for vesicles as σ plays for droplets, hexatic order should lead here to similar effects on the spectrum $\omega(l)$. For vesicles the dynamical fluctuations take place at very small Reynolds numbers [48]. Therefore, the convective and the inertial terms can be neglected in the Navier-Stokes equation (13a) for the surrounding bulk fluid. Thus, here we must solve the Stokes equation

$$\vec{\nabla} p = \eta \nabla^2 \vec{v}, \tag{64}$$

where η and $\vec{v}$ denote now the shear viscosity and the velocity of the bulk fluid, assumed to be the same inside and outside the membrane. The undulating membrane imposes the boundary condition

$$\vec{N} \cdot \vec{v}(\vec{r})|_{\vec{r} = \vec{R}_0(1+\zeta)} = R_0 \dot{\zeta}, \tag{65}$$

where $\vec{R}_0$ is given by Eq. (2) and the membrane velocity by

$$R_0 \dot{\zeta} \equiv R_0 \frac{\partial \zeta(\theta, \varphi, t)}{\partial t}. \tag{66}$$

The following analysis simplifies somewhat by imposing boundary conditions for the components $\vec{\nabla}(\vec{N} \cdot \vec{v})$ and $\vec{\nabla} \times \vec{v}$ instead of v_θ and v_φ. Then,

$$\vec{N} \cdot \vec{\nabla}[\vec{N} \cdot \vec{v}(\vec{r})]|_{\vec{r} = \vec{R}_0(1+\zeta)} = -\vec{\nabla} \cdot (R_0 \dot{\zeta} \vec{N}), \tag{67}$$

$$\vec{N} \cdot [\vec{\nabla} \times \vec{v}(\vec{r})]|_{\vec{r} = \vec{R}_0(1+\zeta)} = 0, \tag{68}$$

where Eq. (67) follows from the condition $\vec{\nabla} \cdot \vec{v} = 0$.

We proceed now as follows [46]. For a given (deformed) vesicle shape the bending forces on its surface are known. These forces must be balanced by the viscous stresses. The induced flow field $\vec{v}$ can be calculated by using Lamb's solution with these boundary conditions. Details about this solution have been given by several authors, cf., e.g., Refs. [46,49,50]. The main formulas are summarized in Appendix D.

As shown in Appendix D, the viscous force $\vec{\Pi} \equiv \Pi_n \vec{N} + \vec{\Pi}_t$ associated with Lamb's solution [see Eqs. (D1) and (D4)] is given by Eqs. (D12), (D13), and (D14). By using Eqs. (D9) and (D10), one then obtains for the normal and tangential force differences

$$\Pi_n^<(x) - \Pi_n^>(x) = \sum_{l=1}^{\infty} \sum_{m=-l}^{l} \dot{r}_{lm}(t)\, \eta \times \frac{(2l+1)(2l^2+2l-3)}{l(l+1)} Y_{lm}(x), \tag{69}$$

and

$$\vec{\Pi}_t^<(x) - \vec{\Pi}_t^>(x) = \sum_{l=1}^{\infty} \sum_{m=-l}^{l} \dot{r}_{lm}(t) R_0 \eta \frac{2l+1}{l(l+1)} \vec{\nabla} Y_{lm}(x), \tag{70}$$

where $\vec{\Pi}_t^<$ and $\vec{\Pi}_t^>$ refer to forces inside and outside of the vesicle, respectively.

The tangential motion of the fluid along the membrane induces lipid flow within the membrane itself. However, the membrane stays locally incompressible. This constraint is

enforced by the local surface tension in Eq. (63), which balances the tangential component of the stress vector. Then, with

$$\sigma(x,t)=\sigma_0+\sum_{l=1}^{\infty}\sum_{m=-l}^{l}\sigma_{lm}(t)\mathrm{Y}_{lm}(x), \tag{71}$$

one finds (for $l\geqslant 1$)

$$\sigma_{lm}(t)=\dot{r}_{lm}(t)R_0\eta\frac{2l+1}{l(l+1)}. \tag{72}$$

Since any nonstationary membrane configuration exerts a local force on the surrounding fluid the shape displacement leads to a generalized pressure discontinuity $\Delta p(x)$ which balances the normal component of the pressure discontinuity between the inside and outside

$$\Pi_n^{<}(x)-\Pi_n^{>}(x)=\Delta p(x), \tag{73}$$

where $\Delta p(x)$ can be expanded in spherical harmonics as in Eq. (19). In order to determine the coefficients p_{lm} in Eq. (19) now the variation of the vesicle free energy has to be calculated. Details are presented in Appendix C.

The deformed surface is characterized by the Gaussian curvature [see Eq. (C14)]

$$G'(x)=\frac{1}{R_0^2}+\frac{1}{R_0^2}\sum_{l,m}(l-1)(l+2)r_{lm}\mathrm{Y}_{lm}(x), \tag{74}$$

and the mean curvature given by Eq. (35). The volume change is given by Eq. (21) and the change in surface area by Eq. (C7), which becomes

$$A'-A=R_0^2\left(2\sqrt{4\pi}r_{00}+\sum_{l=1}^{\infty}\sum_{m=-l}^{l}|r_{lm}|^2[1+l(l+1)/2]\right)+O(r_{lm}^3). \tag{75}$$

The volume constraint can again be implemented by considering displacements which fulfill Eq. (22). Then, upon defining the excess area (relative to a sphere) by $\delta A=A-4\pi R_0^2$, the area constraint reads

$$\frac{1}{2}R_0^2\sum_{l=1}^{\infty}\sum_{m=-l}^{l}|r_{lm}|^2(l-1)(l+2)=\delta A\equiv\text{const}. \tag{76}$$

Similarly, the area term of Eq. (63) for the deformed sphere becomes

$$F_a'=F_a+2R_0^2\sum_{l,m}\sigma_{lm}r_{lm}^*+\frac{1}{2}\sigma_0R_0^2\times\sum_{l=1}^{\infty}\sum_{m=-l}^{l}|r_{lm}|^2(l-1)(l+2). \tag{77}$$

Finally, it has been shown in Refs. [51,52] that the bending energy of a quasispherical vesicle is given by

$$F_b'=F_b+\frac{1}{2}\kappa R_0^2\int dA\,\zeta\mathcal{L}\zeta, \tag{78}$$

where $F_b=8\pi\kappa$ and $\mathcal{L}$ can be evaluated on an undeformed sphere to leading order in ζ,

$$\mathcal{L}=D^iD_iD^jD_j+\frac{2}{R_0^2}D^iD_i. \tag{79}$$

Upon using the decomposition (10) of $\zeta(x,t)$, one finds

$$F_b'=F_b+\frac{1}{2}\kappa\sum_{l=1}^{\infty}\sum_{m=-l}^{l}|r_{lm}|^2l(l+1)(l-1)(l+2). \tag{80}$$

We now insert Eqs. (77), (24), and (80) into Eq. (19) (with $\tilde{F}'$ replacing F_d') and set again $r_{lm}=r_{lm}^0(t)e^{-i\omega(l)t}$. Upon equating the pressure discontinuity in Eq. (19) to the normal force difference (69), we find for the fluctuation spectrum of spherical vesicles with hexatic order (for $l>0$)

$$\omega(l)=-i\frac{\Gamma(l)}{\eta R_0^3}(l-1)(l+2)\times\left[\kappa l(l+1)+\sigma_0R_0^2+K_A\frac{(l-1)(l+2)}{l(l+1)}\right], \tag{81}$$

with

$$\Gamma(l)\equiv\frac{l(l+1)}{(2l+1)(2l^2+2l-1)}. \tag{82}$$

Note that $\omega(l)$ vanishes for $l=1$, corresponding to translations of the vesicle as a whole.

The eigenfrequencies $\omega(l)$ explicitly depend on the $l=0$ component of the tension σ_0 which acts as Lagrange multiplier for the area. Since the value of σ_0 is generally not known, one has to use the area constraint (76) (and the fluctuation-dissipation theorem) to express σ_0 in terms of δA. Which modes pick up the excess area depends on the ratio $\tilde{\gamma}=\sigma R_0^2/\kappa$. As shown in Ref. [47], for floppy membranes (i.e., small $\tilde{\gamma}$) each mode contributes equally to the excess area, whereas for stiff membranes (i.e., large $\tilde{\gamma}$) only the lowest mode ($l=2$) will develop a large amplitude [53].

For the purpose of estimating the effect of hexatic order, we proceed in a different way. The area constraint becomes much easier to handle if the volume constraint can be neglected. By assuming that the vesicle is permeable to both water and larger molecules, the area constraint can be incorporated directly (again to leading order in the r_{lm}'s) by choosing

$$r_{00}=-\frac{1}{2\sqrt{4\pi}}\sum_{l=1}^{\infty}\sum_{m=-l}^{l}|r_{lm}|^2\left(1+\frac{l(l+1)}{2}\right). \tag{83}$$

Then, $A'=A$ and one can set $\sigma_0=0$ in Eq. (81). Equivalently, we focus on floppy vesicles, formed under conditions such that $\sigma R_0^2 \ll \kappa$.

In the flat space limit of $\sigma_0=0$, large R_0 and $l \gg 1$ with $k \equiv l/R_0$ fixed, one has

$$\omega \simeq -i\frac{1}{4\eta}\left[\kappa k^3+\frac{K_A}{R_0^2}k\right]. \tag{84}$$

As for the liquid droplets discussed in Sec. II, the hexatic contribution drops out as $R_0 \to \infty$ and we recover the result for undulation modes of a flat fluid bilayer [54]. The frequency shift (81) depends on the ratio K_A/κ. However, for large vesicles we expect that $K_A \simeq 4\kappa$ (a *universal* result for flat hexatic membranes at long wavelengths [55]) leading to a frequency enhancement in Eq. (81) (with $\sigma_0=0$) by a factor $\simeq 13/9 \simeq 1.44$ for the $l=2$ quadrupole mode. Note the relatively pronounced effect of hexatic order. In general, we expect the largest change in the characteristic frequencies for *floppy* vesicles with $\tilde{\gamma}=\sigma R_0^2/\kappa \ll 1$.

Similar to droplets, the presence of an icosahedral array of defects in hexatic membranes leads to an equilibrium configuration with a deformed surface. For vesicles, the complete first variation of the free energy $\tilde{F}$ [see Eq. (63)] reads

$$\begin{aligned}\delta^{(1)}\tilde{F}=&\frac{1}{2}\kappa\int d^2x\sqrt{g(x)}\{[2H(x)]^2\delta^{(1)}g(x)\\&+8H(x)\delta^{(1)}H(x)\}+\sigma_0\int d^2x\sqrt{g(x)}\delta^{(1)}g(x)\\&+\int d^2x\sqrt{g(x)}p\,\delta^{(1)}V(x)-K_A\int d^2x\sqrt{g(x)}\frac{1}{R_0^2}\\&\times\sum_{l=1}^{\infty}\sum_{m=-l}^{l}\frac{(l-1)(l+2)}{l(l+1)}s_{lm}\mathrm{Y}_{lm}(x)\\&\times\sum_{l',m'}r^*_{l'm'}\mathrm{Y}^*_{l'm'}(x),\end{aligned} \tag{85}$$

where (again) $\delta^{(1)}g$ is given by Eq. (C4), $\delta^{(1)}H$ by Eq. (C16), and $\delta^{(1)}V$ by Eq. (C6). Since integration by parts shows that

$$\int d^2x\sqrt{g(x)}H(x)\nabla^2\zeta(x)=\int d^2x\sqrt{g(x)}\zeta(x)\nabla^2H(x), \tag{86}$$

the equilibrium shape equation for quasispherical vesicles with hexatic order becomes now

$$\begin{aligned}&p+2\sigma_0H(x)-4H(x)\kappa[H^2(x)-G(x)]-2\kappa\nabla^2H(x)\\&\quad=K_A\frac{1}{R_0^3}\sum_{l=1}^{\infty}\sum_{m=-l}^{l}\frac{(l-1)(l+2)}{l(l+1)}\mathrm{Y}_{lm}(x)s_{lm}.\end{aligned} \tag{87}$$

Upon making again the ansatz (32) (where $2H_0\sigma_0+p=0$) and using $G=G_0+2\widetilde{\delta H}/R_0$, one finds for the mean curvature

$$\begin{aligned}2H(x)=&2H_0+\frac{1}{R_0}\sum_{l=1}^{\infty}\sum_{m=-l}^{l}\frac{K_A}{\kappa l(l+1)+\sigma_0R_0^2}\\&\times\frac{(l-1)(l+2)}{l(l+1)}s_{lm}\mathrm{Y}_{lm}(x),\end{aligned} \tag{88}$$

where the static surface deformation coefficients in the ground state are given by

$$r^0_{lm}=s_{lm}\frac{K_A}{\kappa l^2(l+1)^2+\sigma_0R_0^2l(l+1)}, \tag{89}$$

for $l>0$ and $r^0_{lm}=0$ for $l=m=0$.

However, icosahedral symmetry again insures that $s_{lm}=0$, and hence $r^0_{lm}=0$, unless $l=6,10,12,\ldots$, at least for floppy, approximately spherical vesicles. Hence, corrections of order s_{lm} have no influence on the frequencies $\omega(l)$ for small l. Just as for hexatics on liquid droplets, disclination motion is negligible during an undulation period and the dispersion relation (81) remains valid for $0<l<6$. This can be seen by using an estimate similar to that of Sec. II B. Here, $\omega(l=2)\simeq 40$ Hz for a 1 μm vesicle and the disclination diffusion constant is $D_5 \approx (a_0/\xi_T)^2 D_{lipid}$, where $D_{lipid} \simeq 10^{-8}$ cm^2/s and $(a_0/\xi_T)^2 \simeq 10^{-2}$.

Finally, we show that our assumption that the regular part of the bond-angle field relaxes rapidly on the time scale of undulation modes is indeed justified for vesicles with hexatic order. As follows from Eq. (B8) the relaxational dynamics for θ^{reg} is described by

$$\eta_m\frac{d\theta^{reg}}{dt}=K_A\nabla^2\theta^{reg}, \tag{90}$$

where η_m is the shear surface viscosity of the membrane. For simplicity, we have neglected in the last equation defects which are immobile on the time scale of ripples anyhow. Upon expanding θ^{reg} in terms of spherical harmonics

$$\theta^{reg}=\sum_{l=0}^{\infty}\sum_{m=-l}^{l}\theta^{reg}_{lm}(t)\mathrm{Y}_{lm}(x), \tag{91}$$

and setting

$$\theta^{reg}_{lm}=\theta^0_{lm}e^{-i\omega_\theta(l)t}, \tag{92}$$

one finds

$$\omega_\theta(l)=-i\frac{K_A}{\eta_mR_0^2}l(l+1). \tag{93}$$

Thus, by comparing with the undulation spectrum ω given by Eq. (81) one obtains with $\eta_m=\eta h$ (where $h \simeq 100-1000$ nm for bilayers) for floppy vesicles and large l,

$$\frac{\omega(l)}{\omega_\theta(l)} \simeq \frac{\kappa}{4K_A}\frac{h}{R_0}l. \tag{94}$$

Thus, $\omega(l) \ll \omega_\theta(l)$ for $h \ll R_0$, justifying our assumption for large vesicles. Similar arguments apply to spherical droplets and bubbles and cylindrical geometries.

VI. EXPERIMENTAL CONSEQUENCES

We conclude by discussing the implications of our results for possible experiments. As discussed in the Introduction, one of our main motivations was to search for dynamic signatures of hexatic order in curved geometries, order which is difficult to detect by other means. As shown in Sec. V, the frequency shift due to hexatic order is particularly large for vesicles. The $l=2$ quadrupole relaxation rate can be enhanced by a factor $\simeq 1.44$ due to bond-orientational order and should be experimentally detectable by measuring the decay rate of fluctuations by, e.g., video or fluorescence microscopy [46].

For liquid droplets the influence of hexatic order on the fluctuation spectrum is somewhat weaker. For the magnitude of the hexatic stiffness one has the estimate [1]

$$K_A = C(T)\left(\frac{\xi_T}{a_0}\right)^2, \tag{95}$$

where a_0 is the lattice constant, ξ_T is a translational correlation length which diverges as T approaches T_m, and $C(T)$ is a prefactor. When $T \gg T_m$ one has $C(T) \simeq 2E_c(a/a_0)^2$ [1], where E_c is the energy of a dislocation core with diameter $a \approx a_0$. On the other hand, for the liquid metal droplets $\sigma \simeq k_B T/a_0^2$ and with $C(T) \simeq k_B T$ one has $K_A/\sigma R_0^2 \simeq 1$ for $\xi_T \simeq R_0$. Thus, hexatic order should also have experimentally relevant consequences for the fluctuation spectrum of liquid droplets and cylinders when the translational correlation length grows to become comparable to the sphere size or cylinder radius. As we saw in Sec. III, the Plateau-Rayleigh instability will also be modified for $K_A \neq 0$. As the liquid cylinder decays into a chain of droplets the distance between the droplets will depend on the ratio $K_A/\sigma R_0^2$, as follows from Eq. (52). For $K_A/\sigma R_0^2 \simeq 1$ one has $\lambda_f = 2\pi/k_f \simeq 12.6 R_0$ as typical distance between the droplets in contrast to $\lambda_f \simeq 9.0 R_0$ appropriate to $K_A = 0$ [39,40].

For multielectron bubbles σ is determined by the distance b_0 between the helium atoms. Here, we expect that $\sigma \simeq 3k_B T_m/b_0^2$, where T_m is the melting temperature and $b_0 \simeq 3$ Å for liquid helium. From the experiments by Grimes and Adams [4] it is known that for the planar case the dimensionless ratio $\Gamma_m \equiv (e^2\sqrt{\pi n}/k_B T_m) \simeq 140$ and $T_m = 0.73$ K for a charge density $n = 10^9$ cm^{-2}. Thus, for ^{4}He one has $\sigma \simeq 3 \times 10^{-4}$ J/m^2 at $T \approx T_m$. For helium bubbles with $N \simeq 10^6$ one has $a_0 = (4\pi R_{cl}^2/N)^{1/2} \simeq 300$ Å and the critical radius $R_{cl} \simeq 10$ μm. By using the $T=0$ result $E_c \simeq 0.1 e^2/a_0$ [7] one finds $K_A/\sigma R_{cl}^2 \simeq 10^{-4}$. It is worth mentioning that $K_A/\sigma R_{cl}^2 \sim 1/\sqrt{N}$, since $K_A \sim N E_c$ and $E_c \sim R_{cl}^2/N^{3/2}$. Thus, the influence of hexatic order will be somewhat stronger for bubbles with smaller N.

Thus, hexatic order has only a weak influence on the stability of multielectron bubbles. But with sophisticated experimental setups it still might be possible to measure its effects. A possible scenario to study fission could, e.g., make use of the fact that bubbles become compactified as they move under the influence of an external field away from the liquid-vapor interface towards the positive electrode immersed in the liquid. Thus, if for $T > T_i$ multielectron bubbles with an initial radius R_0 are stable to fission up to a distance h from the interface then they will be observed at a somewhat larger distance $h + \delta h$ for $T_m < T < T_i$.

It also might be possible to experimentally confirm our theoretical predictions in the regime of stable bubbles by measuring the characteristic frequencies of an oscillating bubble which is stabilized by the balance of bouancy and electric field forces at a constant height below the surface. Our predictions also apply to multi-ion bubbles which experimentally can be realized by charging helium films with ions instead of electrons [20].

Finally, for charged droplets in Paul traps similar effects should be observable by, e.g., trapping a droplet and shooting charges on it until it undergoes fission. For this purpose it might be necessary to use more conventional liquids and to perform the experiments at much higher temperatures. Fission with ordered ions on droplets can still be achieved by using ions with high charge Ze since $T_m \propto Z^2 e^2 \sqrt{n}$. For example, for droplets with $R_0 \simeq 10$ μm and $N \simeq 10^6$ the melting transition should occur at room temperature for $Z=7$. Provided the surface tension of the liquid is large enough the droplets will still be stable at these parameter values.

In summary, we have shown that two-dimensional hexatic order should lead to experimentally observable effects in a variety of systems with spherical and cylindrical geometry. Similar effects could also occur in related systems such as, e.g., cylindrical vesicles. Here, we expect that the laser-induced pearling instability will be modified by the presence of hexatic order [56,57].

Crystalline order will also alter the fluctuation spectrum of spherical and cylindrical droplets and membranes [58–60]. The effects discussed here should be even *larger* if the hexatic phase is bypassed and one freezes directly into a two-dimensional solid with shear modulus μ. The resulting frequency shifts can be estimated by replacing K_A by μR_0^2 in the formulas above. Details will be given in an upcoming publication [45].

ACKNOWLEDGMENTS

We thank S. Balibar, G. Gabrielse, N. Goddard, J. Lidmar, and R. Pindak for helpful discussions. This work has been supported by the NSF through Grant No. DMR97-14725 and through the Harvard MRSEC via Grant No. DMR98-09363. P.L. acknowledges support by the Deutsche Forschungsgemeinschaft (LE 1214/1-1).

APPENDIX A: PARAMETRIZATION OF SHAPE

Here, we review the elementary differential geometry needed to determine all relevant geometrical properties, i.e.,

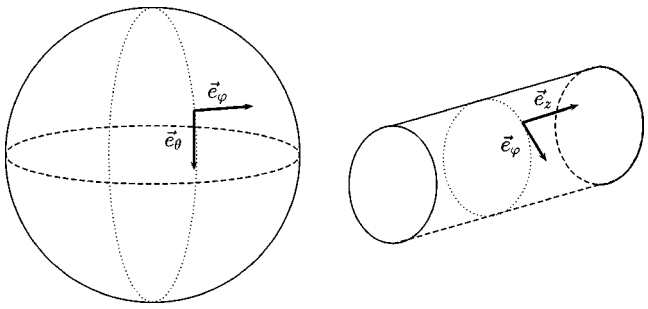

FIG. 5. Orthonormal basis vectors $\vec{e}_\theta$ and $\vec{e}_\varphi$ of the tangential plane of the sphere and basis vectors $\vec{e}_\varphi$ and $\vec{e}_z$ of the tangential plane of the cylinder. One has $\vec{e}_\theta=\vec{R}_1/R_0$, $\vec{e}_\varphi=\vec{R}_2/R_0 \sin\theta$ for the sphere, see Eq. (2). For the cylinder, $\vec{e}_\varphi=\vec{R}_1/R_0$ and $\vec{e}_z=\vec{R}_2$, see Eq. (37).

the first and second fundamental forms, of a surface in terms of its surface vector $\vec{R}$. For a more extensive review, see Ref. [61]. For simplicity, we specialize here to spherical and cylindrical surfaces. *Deformations* of these shapes are treated in Appendix C.

For an undeformed sphere with constant radius R_0 one can choose $x=(x^1,x^2)\equiv(\theta,\varphi)$ with polar coordinates θ and φ. The surface vector is then given by

$$\vec{R}(\theta,\varphi)=R_0(\sin\theta\cos\varphi,\sin\theta\sin\varphi,\cos\theta). \tag{A1}$$

The first fundamental form is defined by

$$g_{ij}\equiv\vec{R}_i\cdot\vec{R}_j, \tag{A2}$$

with the covariant vectors

$$\vec{R}_j\equiv\vec{R}_{,j}\equiv\partial_{sj}\vec{R}\equiv\frac{\partial\vec{R}}{\partial s^j}. \tag{A3}$$

On the sphere the vectors $\{\vec{R}_1(x),\vec{R}_2(x)\}$ form an orthogonal (but not orthonormal) basis in the tangential plane at the point x, cf. Fig. 5. The contravariant components are given by $\vec{R}^k=g^{ki}\vec{R}_i$, where g^{ij} is the inverse of g_{ij}, i.e., $g^{ij}g_{jk}=\delta^i_k$. We use the summation convention throughout. With the parametrization of Eq. (A1), we have

$$\vec{R}_1=R_0(\cos\theta\cos\varphi,\cos\theta\sin\varphi,-\sin\theta),$$

$$\vec{R}_2=R_0(-\sin\theta\sin\varphi,\sin\theta\cos\varphi,0). \tag{A4}$$

The area element is generally given by $dA=\sqrt{g}dx^1dx^2$, where

$$g\equiv\det(g_{ij}). \tag{A5}$$

For a sphere the first fundamental form is given by

$$(g_{ij})=\begin{pmatrix}R_0^2 & 0\\ 0 & R_0^2\sin^2\theta\end{pmatrix} \tag{A6}$$

and $dA=R_0^2\sin\theta d\theta d\varphi$.

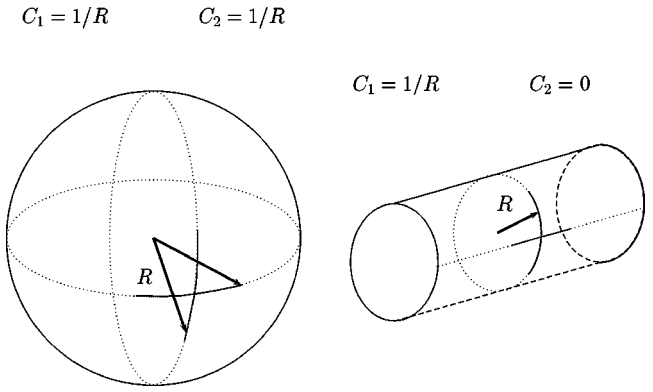

FIG. 6. Principal curvatures for spheres and cylinders. In both cases the principal directions of curvature are drawn. For a sphere both principal curvatures are identical, i.e., $C_1=C_2=1/R$. For a cylinder one has $C_1=1/R$, $C_2=0$. The principal curvatures are the eigenvalues of $(-b^j_i)$. Thus, $2H=-(C_1+C_2)$ and $G=C_1C_2$.

The mean curvature H and the Gaussian curvature G are determined by the *second* fundamental form, which is defined by

$$b_{ij}\equiv\vec{R}_{ij}\cdot\vec{N}=-\vec{R}_i\cdot\vec{N}_j, \tag{A7}$$

where $\vec{N}$ is the (local) unit normal vector to the surface

$$\vec{N}(x^1,x^2)\equiv\frac{\vec{R}_1(x^1,x^2)\times\vec{R}_2(x^1,x^2)}{\sqrt{g}}, \tag{A8}$$

and the second equality of Eq. (A7) follows from $\vec{R}_i\cdot\vec{N}=0$. In terms of the second fundamental form, and upon raising an index of b_{ij} via the operation $g^{ik}b_{kj}\equiv b^i_j$, we have

$$2H=-b^i_i \quad\text{and}\quad G=\det(b^i_j)=\frac{b}{g}\equiv\frac{\det(b_{ij})}{\det(g_{ij})}. \tag{A9}$$

See Fig. 6. For a sphere one has

$$\vec{N}=\frac{\vec{R}}{R_0}=(\sin\theta\cos\varphi,\sin\theta\sin\varphi,\cos\theta) \tag{A10}$$

and the second fundamental form becomes

$$(b_{ij})=\begin{pmatrix}-R_0 & 0\\ 0 & -R_0\sin^2\theta\end{pmatrix}. \tag{A11}$$

It is easy to check that $b^i_j=-\delta^i_j/R_0$ and hence, $H=1/R_0$ and $G=1/R_0^2$ in this case.

The covariant derivative of a vector with covariant components a_i and contravariant components a^j is defined by [62]

$$D_ia_j=a_{j,i}-a_k\Gamma^k_{ij} \quad\text{and}\quad D_ia^j=a^j_i+a^k\Gamma^j_{ki}. \tag{A12}$$

Here, the Γ^k_{ij} are the Christoffel symbols of the second kind. They are related to the Christoffel symbols of the first kind Γ_{ikj} by $\Gamma^k_{ij}=g^{kl}\Gamma_{ilj}$, where

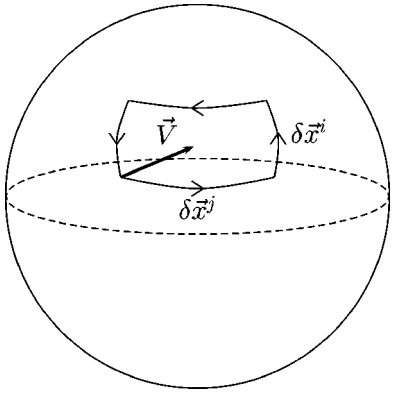

FIG. 7. Geometrical interpretation of the Riemann curvature tensor on the sphere. Parallel transport of the vector $\vec{V}$ along the path shown in the figure leads to a rotation $(\vec{V}'-\vec{V})^l = R^l_{kji} V^k \delta x^j \delta x^i$, where R^l_{kji} is the Riemann curvature tensor, defined in Eq. (A17). As a consequence, on a curved surface covariant derivatives do not commute. Indeed, $[D_i, D_j]\eta^i = G\eta_j$, where G is the Gaussian curvature which in two dimensions determines all components of R^l_{kji}.

$$\Gamma_{ikj} \equiv \frac{1}{2}(\partial_i g_{kj} + \partial_j g_{ik} - \partial_k g_{ij}). \tag{A13}$$

Note that the Γ_{ikj} are symmetric in the first and last index, i.e.,

$$\Gamma_{ikj} = \Gamma_{jki}. \tag{A14}$$

For a sphere with polar coordinates, we have

$$\Gamma^{\theta}_{\theta\theta} = \Gamma^{\varphi}_{\theta\theta} = \Gamma^{\theta}_{\theta\varphi} = \Gamma^{\varphi}_{\varphi\varphi} = 0, \quad \Gamma^{\varphi}_{\theta\varphi} = \frac{\cos\theta}{\sin\theta},$$

$$\Gamma^{\theta}_{\varphi\varphi} = -\sin\theta\cos\theta. \tag{A15}$$

As can be shown by a direct calculation, the covariant derivatives of g_{ij}, g^{ij}, and δ^i_j vanish. Covariant derivatives do not commute, in general. For scalars one has $D_i D_j f = D_j D_i f$ if $\partial_i \partial_j f = \partial_j \partial_i f$. However, for vectors the commutator of covariant derivatives is given by

$$[D_i, D_j] a_k = a_l R^l_{kji}. \tag{A16}$$

Here, R^l_{kji} is the (mixed) Riemann curvature tensor

$$R^l_{kji} \equiv \partial_j \Gamma^l_{ki} - \partial_i \Gamma^l_{kj} + \Gamma^m_{ki}\Gamma^l_{mj} - \Gamma^m_{kj}\Gamma^l_{mi}. \tag{A17}$$

In two spatial dimensions one has a particularly simple relation

$$R^l_{kji} = g_{km}\gamma^{lm}\gamma_{ji} G, \tag{A18}$$

where γ^{ij} is the antisymmetric contravariant tensor,

$$\gamma^{ij} \equiv (\delta^i_1 \delta^j_2 - \delta^i_2 \delta^j_1)/\sqrt{g}, \tag{A19}$$

with covariant counterpart $\gamma_{kl} = \gamma^{ij} g_{ik} g_{jl}$. Note, Eq. (A18) shows that the Gaussian curvature is determined by the first fundamental form only. This is the content of the famous theorema egregium of Gauss. A geometrical interpretation of the Riemann curvature tensor is given in Fig. 7.

For a sphere the nonzero components of the Riemann curvature tensor are

$$R^1_{212} = -R^1_{221} = \frac{b}{g_{11}} = \sin^2\theta, \quad -R^2_{112} = R^2_{121} = \frac{b}{g_{22}} = 1. \tag{A20}$$

Covariant derivatives have another useful property; integrals over covariant derivatives of vector fields can be integrated by parts, similar to vector fields in flat space. This is the content of the divergence theorem: for an arbitrary closed surface M (i.e., a surface with no boundary, $\partial M = 0$) one has

$$\int_M dA D_i v^i = 0, \tag{A21}$$

for any vector v^i. Here, $D_i v^i = (1/\sqrt{g})\partial_i(\sqrt{g} v^i) \equiv \vec{\nabla}\cdot\vec{v}$ is the divergence of $\vec{v}$ on a curved surface. Finally, the Laplacian is defined by $\Delta = D^i D_i$. It becomes on the sphere

$$\Delta_{sph} = \frac{1}{R_0^2}\left\{ \frac{1}{\sin^2\theta}\frac{\partial^2}{\partial\varphi^2} + \frac{1}{\sin\theta}\frac{\partial}{\partial\theta}\left(\sin\theta\frac{\partial}{\partial\theta}\right)\right\}. \tag{A22}$$

Note that the eigenfunctions of Δ_{sph} are spherical harmonics

$$\Delta_{sph} Y_{lm} = \frac{-l(l+1)}{R_0^2} Y_{lm}. \tag{A23}$$

For undeformed cylinders with radius R_0 one can choose $x = (\varphi, z)$. The surface vector is then given by

$$\vec{R}(x) = (R_0\cos\varphi, R_0\sin\varphi, z). \tag{A24}$$

Here, the first fundamental form is given by

$$(g_{ij}) = \begin{pmatrix} R_0^2 & 0 \\ 0 & 1 \end{pmatrix} \tag{A25}$$

and $dA = R_0 d\varphi dz$.

The second fundamental form becomes

$$(b_{ij}) = \begin{pmatrix} -R_0 & 0 \\ 0 & 0 \end{pmatrix}. \tag{A26}$$

Thus, $G_0 = 0$ and $H_0 = 1/2R_0$.

Since for cylinders g_{ij} is independent of φ and z all Christoffel symbols vanish, i.e., $\Gamma^k_{ij} = 0$. Thus, $\partial_i = D_i$ and the Laplacian becomes for this geometry

$$\Delta_{cyl} = \partial^i \partial_i = \frac{1}{R_0^2}\frac{\partial^2}{\partial\varphi^2} + \frac{\partial^2}{\partial z^2}. \tag{A27}$$

The eigenfunctions are plane waves

$$\Delta_{cyl} e^{ikz} e^{im\varphi} = -\frac{1}{R_0^2}(k^2 R_0^2 + m^2) e^{ikz} e^{im\varphi}. \quad \text{(A28)}$$

APPENDIX B: HEXATIC FREE ENERGY

In this appendix, we derive a useful representation of the hexatic free energy for vesicles, droplets and multielectron bubbles. The discussion is kept rather general since it has to be valid for both deformed and undeformed spheres and cylinders. The discussion here generalizes earlier approaches [28,55] to (arbitrary) curved geometries with defects. See also Ref. [35].

Consider, the free energy F_h introduced in Sec. II, i.e.,

$$F_h = \frac{1}{2} K_A \int d^2x \sqrt{g} D_i n^j D^i n_j . \quad \text{(B1)}$$

We now introduce an ortho*normal* basis $\{\vec{e}_\alpha\}$ of the tangential space. (Note that orthonormality is not guaranteed for the tangent basis vectors discussed in Appendix A; for example, the "natural" basis vectors $\vec{R}_\theta$ and $\vec{R}_\varphi$ for the sphere are merely orthogonal.) Then, for an arbitrary vector field $\vec{V}$ one has the contravariant components

$$\vec{V} = V^\alpha \vec{e}_\alpha , \quad \vec{e}_\alpha \cdot \vec{e}_\beta = \delta_{\alpha\beta} . \quad \text{(B2)}$$

Here, Greek indices have been used to distinguish this basis from the $\{\vec{R}_i\}$. The covariant derivative of $\vec{V}$ is now given in terms of

$$D_i V_\alpha = \vec{e}_\alpha \cdot (\partial_i \vec{V}), \quad \text{(B3)}$$

so that

$$D_i V_\alpha = \partial_i V_\alpha - \omega_{i\beta\alpha} V^\beta, \quad \text{(B4)}$$

with $V_\alpha = V^\beta \vec{e}_\beta \cdot \vec{e}_\alpha$ and

$$\omega_{i\beta\alpha} = \vec{e}_\beta \cdot \partial_i \vec{e}_\alpha \quad \text{(B5)}$$

is the affine connection appropriate for this basis [63]. For orthonormal $\vec{e}_\alpha$ one has $\omega_{i\beta\alpha} = -\omega_{i\alpha\beta}$. Thus, one can define a covariant vector field A_i by

$$\omega_{i\alpha\beta} = \varepsilon_{\alpha\beta} A_i , \quad \text{(B6)}$$

where $\varepsilon_{\alpha\beta} \equiv \delta^1_\alpha \delta^2_\beta - \delta^2_\alpha \delta^1_\beta$ is the Levi-Civita symbol.

We now set, $\vec{n} = n^\alpha \vec{e}_\alpha$. Since $n^i n_i = n^\alpha n_\alpha = 1$ it is possible to introduce an bond-angle field Θ as angle between $\vec{n}$ and the local reference frame $\{\vec{e}_\alpha\}$with

$$n_{\alpha=1} = \cos\Theta , \quad n_{\alpha=2} = \sin\Theta . \quad \text{(B7)}$$

Then, $\partial_i n_\alpha = \varepsilon_{\alpha\beta} n^\beta \partial_i \Theta$, and it is easy to show that Eq. (B1) becomes

$$F_h = \frac{1}{2} K_A \int d^2x \sqrt{g(x)} (D^i\Theta + A^i)(D_i\Theta + A_i). \quad \text{(B8)}$$

For sixfold bond-oriented order, we identify θ with $\theta + 2\pi/6$, which determines the minimum charge of disclination defects. The vector field A_i is a "vector potential" associated with the Gaussian curvature, i.e.,

$$D_i A_j - D_j A_i = \partial_i A_j - \partial_j A_i = -G(x)\gamma_{ij} , \quad \text{(B9)}$$

see Ref. [61]. The last result is a consequence of Eq. (A18) and of the representation of the curvature tensor in this basis, namely,

$$R^\alpha_{\beta ji} = \partial_j \omega^\alpha_{\beta i} - \partial_i \omega^\alpha_{\beta j} + \omega^\gamma_{\beta i} \omega^\alpha_{\gamma j} - \omega^\gamma_{\beta j} \omega^\alpha_{\gamma i} . \quad \text{(B10)}$$

Note that Eq. (B9) allows an explicit construction for the vector potential for an arbitrary closed surface with a given Gaussian curvature, that is,

$$A_j(x) = -g^{kl} \gamma_{lj} D_k(x) \int d^2x' \sqrt{g(x')} \Gamma_g(x,x') G(x'). \quad \text{(B11)}$$

Here, $\Gamma_g(x,x')$ is the Green's function for the Laplacian Δ_g,

$$\Delta_g \Gamma_g(x,x') = \frac{\delta(x-x')}{\sqrt{g}} . \quad \text{(B12)}$$

Note that the Laplacian Δ_g depends explicitly on the metric g, since

$$\Delta_g f \equiv D^i D_i f = \frac{1}{\sqrt{g}} \partial_i (\sqrt{g} \partial^i f). \quad \text{(B13)}$$

We now divide the field Θ into a regular part Θ^{reg} and a singular part Θ^{sing} which represents the contribution of defects. The regular part Θ^{reg} fulfills $D_i D_j \Theta^{reg} = D_j D_i \Theta^{reg}$; we assume that this part relaxes rapidly on the time scale of shape deformations. The singular part Θ^{sing} is related to the disclination density $s(x)$ by [cf. Eq. (5)]

$$\gamma^{ij} D_i D_j \Theta^{sing} = s(x) \equiv \frac{1}{\sqrt{g}} \sum_i q_i \delta(x - x_i), \quad \text{(B14)}$$

where $q_i = \pm 2\pi/6$ for disclinations in a hexatic. Thus,

$$D_j(x) \Theta^{sing}(x) = g^{kl} \gamma_{lj} D_k(x) \int d^2x' \sqrt{g(x')} \Gamma_g(x,x') s(x'), \quad \text{(B15)}$$

where $\Gamma_g(x,x')$ is the same Green's function as in Eq. (B11). Note that in the gauge defined by Eq. (B11), one has

$$D_i D^i \Theta^{sing} + D_i A^i = 0, \quad \text{(B16)}$$

which is the Euler-Lagrange equation of the functional (B8).

By using Eqs. (B11) and (B15) the hexatic free energy (B8) becomes for an arbitrary manifold with metric g and Gaussian curvature $G(x)$

$$F_h = -\frac{1}{2}K_A \int d^2x \sqrt{g(x)} \int d^2x' \sqrt{g(x')}[G(x)-s(x)] \times \Gamma_g(x,x')[G(x')-s(x')], \tag{B17}$$

where we have integrated by parts and used Eq. (B12).

In the planar case, the ground state has no defects, i.e., $s(x)=0$. Then, using $\Gamma_g(x,x')=(1/\Delta)_{x,x'}$, Eq. (B17) reduces to the Liouville action

$$F_h = -\frac{1}{2}K_A \int d^2x \sqrt{g(x)} \int d^2x' \sqrt{g(x')} G(x) \times \left(\frac{1}{\Delta_{xx'}}\right) G(x'). \tag{B18}$$

APPENDIX C: FREE ENERGY OF DEFORMED SPHERES AND CYLINDERS

As the spherical shape gets displaced its free energy changes. In this appendix, we calculate the corresponding contributions arising from (i) the interfacial free energy and the bending energy (Sec. C 1), (ii) the hexatic free energy (Sec. C 2), and (iii) the Coulomb energy (Sec. C 3). We begin by discussing the geometrical properties associated with shape deformations.

1. Geometrical properties and variations of the mean and Gaussian curvature

The displacement of spherical shapes parameterized by Eq. (8) leads to new tangent vectors

$$\vec{R}_i' = \vec{R}_i - R_0\zeta b_i^k \vec{R}_k + R_0\zeta_i \vec{N} \tag{C1}$$

$$= \vec{R}_i(1+\zeta) + R_0\zeta_i \vec{N}. \tag{C2}$$

The first fundamental form then changes according to

$$\delta g_{ij} \equiv g_{ij}' - g_{ij} = \vec{R}_i' \cdot \vec{R}_j' - \vec{R}_i \cdot \vec{R}_j = -2R_0\zeta b_{ij} - R_0\zeta^2 b_{ij} + R_0^2 \zeta_i \zeta_j. \tag{C3}$$

Correspondingly, the change in the area element is given by

$$\sqrt{g+\delta g} = \sqrt{g}\left(1 + 2HR_0\zeta + GR_0^2\zeta^2 + \frac{1}{2}R_0^2\zeta^i\zeta_i\right) + O(\zeta^3) \tag{C4}$$

$$= \sqrt{g}\left(1 + 2\zeta + \zeta^2 + \frac{1}{2}R_0^2\zeta^i\zeta_i\right) + O(\zeta^3). \tag{C5}$$

The volume change is given by

$$\delta V = \int dA R_0(\zeta + HR_0\zeta^2) + O(\zeta^3), \tag{C6}$$

while the area of the deformed sphere is

$$A' = \int d^2x \sqrt{g+\delta g}. \tag{C7}$$

The spherical harmonic decomposition (10) together with Eqs. (C5) and (22) then leads to Eq. (23).

The change in the second fundamental form has only to be known up to first order in ζ. The normal vector of the deformed sphere is given by

$$\vec{N}' = \vec{N} - R_0\zeta^i \vec{R}_i + O(\zeta^2). \tag{C8}$$

Therefore, the second fundamental form changes according to

$$(b_{ij})' = \vec{R}_{ij}' \cdot \vec{N}' = b_{ij} + R_0 D_j\zeta_i + \zeta b_{ij} + O(\zeta^2). \tag{C9}$$

With

$$(g^{jk})' = g^{jk} + 2R_0\zeta b^{jk} + O(\zeta^2), \tag{C10}$$

one finds

$$(b_i^j)' = -\frac{1}{R_0}\delta_i^j(1-\zeta) + R_0 D^j\zeta_i + O(\zeta^2). \tag{C11}$$

The resulting Gaussian curvature of the deformed surface is given by

$$G' = \det(b_i^j{}') = \frac{b'}{g'} = \frac{\det(b_{ij}')}{g+\delta g} + O(\zeta^2). \tag{C12}$$

Therefore,

$$G'(x) - G(x) = -2R_0 HG\zeta + R_0\gamma^{ik}\gamma^{jl}b_{ij}D_l\zeta_k + O(\zeta^2) \tag{C13}$$

$$= -2G\zeta - \nabla^2\zeta + O(\zeta^2), \tag{C14}$$

which leads, upon expanding $G(x)$ and $\zeta(x)$ in spherical harmonics, to Eq. (74).

Similarly, the mean curvature of the deformed surface is given by

$$-2H' = (b_i^i)' = (g^{ij})'(b_{ij})' = (g^{ij}+\delta g^{ij})(b_{ij}+\delta b_{ij}) + O(\zeta^2). \tag{C15}$$

Therefore,

$$2H' = 2H - 2R_0\zeta(2H^2 - G) - R_0 D^i\zeta_i + O(\zeta^2), \tag{C16}$$

which leads via spherical harmonics to Eq. (35).

Although not derived here, Eqs. (C1), (C4), (C6), (C13), and (C16) actually hold for *general* geometries with mean curvature $H(x)$ and Gaussian curvature $G(x)$. These formulas will be needed in the analysis of Secs. II B, III, and V.

2. Hexatic free energy

Next, we calculate the change in hexatic free energy. Since Eq. (B17) holds for arbitrary manifolds one has for the deformed sphere

$$F_h' = -\frac{1}{2}K_A \int d^2x \sqrt{g+\delta g} \int d^2x' \sqrt{g+\delta g} \times [G'(x)-s'(x)]\Gamma_{g+\delta g}(x,x')[G'(x')-s'(x')]. \tag{C17}$$

Here, $\Gamma_{g+\delta g}(x,x')$ is the inverse Laplacian defined on the deformed sphere, i.e.,

$$\Delta_{g+\delta g}\Gamma_{g+\delta g}(x,x') = \frac{\delta(x-x')}{\sqrt{g+\delta g}}. \tag{C18}$$

Furthermore, G' is given by Eq. (C14). As the surface gets displaced the position of the defects might change. This can be taken into account by introducing a disturbed defect distribution

$$s'(x) = s(x) + \frac{1}{R_0^2}\sum_{l=0}^{\infty}\sum_{m=-l}^{l} \delta s_{lm} \mathrm{Y}_{lm}(x) = G_0 + \frac{1}{R_0^2}\left(\delta s_{00} Y_{00}(x) + \sum_{l=1}^{\infty} [s_{lm}+\delta s_{lm}]\mathrm{Y}_{lm}(x)\right). \tag{C19}$$

The coefficient δs_{00} is determined by disclination ''charge conservation,'' i.e.,

$$\int d^2x \sqrt{g+\delta g} s'(x) = 4\pi. \tag{C20}$$

Thus,

$$\delta s_{00} = -2r_{00}. \tag{C21}$$

Since the coefficients δs_{lm} are of order ζ, $s'(x)$, and $G'(x)$ differ only in order ζ. Therefore, one can replace in Eq. (C17) $\sqrt{g+\delta g}$ by $\sqrt{g}$ and $\Gamma_{g+\delta g}(x,x')$ by $\Gamma_g(x,x')$. Since for the sphere [35]

$$\Gamma(x',x'') = -\sum_{l=1}^{\infty}\sum_{m=-l}^{l} \frac{\mathrm{Y}_{lm}(\theta',\varphi')\mathrm{Y}^*_{lm}(\theta'',\varphi'')}{l(l+1)}, \tag{C22}$$

one finally gets

$$F_h' = \frac{1}{2}K_A \sum_{l=1}^{\infty}\sum_{m=-l}^{l} \frac{|r_{lm}(l-1)(l+2)-(s_{lm}+\delta s_{lm})|^2}{l(l+1)} + O(\zeta^2 s_{lm}), \tag{C23}$$

a result needed in Secs. II and V.

3. Coulomb energy

The force (per unit area) acting on a dielectric (with dielectric constant ε) contributed by an arbitrary electric field $\vec{E}$ is given by [27]

$$p = \frac{E^2}{\varepsilon 8\pi}. \tag{C24}$$

Then, in terms of the electrostatic potential ψ, $\vec{E} = -\vec{\nabla}\psi$ with $\nabla^2\psi = 0$, and one can make the ansatz [for $r > R_0(1+\zeta)$]

$$\psi = \frac{eN}{r} + \sum_{l,m} c_{lm}\mathrm{Y}_{lm}\left(\frac{R_0}{r}\right)^{l+1}. \tag{C25}$$

The liquid-vapor interface has to be a surface of constant potential. Thus, $\psi(r = R_0 + R_0\zeta) = \text{const}$. Upon setting $c_{lm} = c r_{lm}$, where c is a constant, one then finds

$$c_{lm} = \frac{eN}{R_0} r_{lm} \tag{C26}$$

and

$$\vec{E} = -\vec{e}_r \frac{\partial}{\partial r}\bigg|_{r=R_0+\zeta R_0} \psi(r) = \frac{eN}{R_0^2}\left(1 + \sum_{l,m}(l-1) r_{lm}\mathrm{Y}_{lm}\right)\vec{e}_r. \tag{C27}$$

Thus,

$$p = \frac{(eN)^2}{8\pi R_0^4 \varepsilon}\left(1 + 2\sum_{l,m}(l-1) r_{lm}\mathrm{Y}_{lm} + O(r_{lm}^2)\right). \tag{C28}$$

APPENDIX D: LAMB'S SOLUTION FOR SPHERICAL RIPPLES

Here, we present the main features of Lamb's solution for obtaining the fluid velocity fields from the surface stresses. We follow here closely the presentations in Refs. [46,49,50], where more details can be found.

The inner solution [i.e., for $r < R_0(1+\zeta)$] of the Stokes equation (64) with viscosity η is given by

$$\vec{v}^{<} = \sum_{l=1}^{\infty}\left(\vec{\nabla}\varphi_l^{<} + \frac{l+3}{2\eta(l+1)(2l+3)} r^2 \vec{\nabla} p_l^{<} - \frac{l}{\eta(l+1)(2l+3)}\vec{r} p_l^{<}\right), \tag{D1}$$

with the velocity potential function

$$\varphi_l^{<}(r,x,t) = \sum_{m=-l}^{l} \varphi_{lm}^{<}(t)\mathrm{Y}_{lm}(x)\left(\frac{r}{R_0}\right)^l, \tag{D2}$$

and the hydrostatic pressure $p_< = \Sigma_l p_l^{<}(r,x,t)$ with

$$p_l^<(r,x,t)=\sum_{m=-l}^{l} p_{lm}^<(t)\mathrm{Y}_{lm}(x)\left(\frac{r}{R_0}\right)^l. \tag{D3}$$

The outer solution can be obtained by performing the replacement $l\rightarrow -(l+1)$ in the formulas above. Thus,

$$\vec{v}^>=\sum_{l=1}^{\infty}\left(\vec{\nabla}\varphi_l^> -\frac{l-2}{2\eta l(2l-1)}r^2\vec{\nabla}p_l^> +\frac{l+1}{\eta l(2l-1)}\vec{r}p_l^>\right). \tag{D4}$$

Here,

$$\varphi_l^>(r,x,t)=\sum_{m=-l}^{l}\varphi_{lm}^>(t)\mathrm{Y}_{lm}(x)\left(\frac{R_0}{r}\right)^{l+1} \tag{D5}$$

and

$$p_l^>(r,x,t)=\sum_{m=-l}^{l} p_{lm}^>(t)\mathrm{Y}_{lm}(x)\left(\frac{R_0}{r}\right)^{l+1}. \tag{D6}$$

The boundary conditions become

$$\vec{N}\cdot\vec{v}(\vec{r})|_{\vec{r}=\vec{R}_0(1+\zeta)}=\sum_{l,m}\left\{\frac{l}{2\eta(2l+3)}R_0p_{lm}^<(t) +\frac{l}{R_0}\varphi_{lm}^<(t)\right\}\mathrm{Y}_{lm}(x) \tag{D7}$$

and

$$\vec{N}\cdot\vec{\nabla}[\vec{N}\cdot\vec{v}(\vec{r})]-\vec{\nabla}\cdot\vec{v}(\vec{r})|_{\vec{r}=\vec{R}_0(1+\zeta)} =\sum_{l,m}\left\{\frac{l(l+1)}{2\eta(2l+3)}p_{lm}^<(t)+\frac{1}{R_0^2}l(l-1)\varphi_{lm}^<(t)\right\}\mathrm{Y}_{lm}(x). \tag{D8}$$

By comparing Eqs. (D7) and (D8) with the right hand sides of Eqs. (65) and (67) one then obtains

$$p_{lm}^<=-\dot{r}_{lm}\eta\frac{(2l+3)(l-1)}{l},\quad p_{lm}^>=\dot{r}_{lm}\eta\frac{(2l-1)(l+2)}{l+1} \tag{D9}$$

and

$$\varphi_{lm}^<=\dot{r}_{lm}R_0^2\frac{(l+1)}{2l},\quad \varphi_{lm}^>=\dot{r}_{lm}R_0^2\frac{l}{2(l+1)}. \tag{D10}$$

The stress vector associated with this velocity field is given by

$$\vec{\Pi}=\Pi_n\vec{N}+\vec{\Pi}_t=-\vec{N}p+\eta\left(\frac{\partial\vec{v}}{\partial r}-\frac{\vec{v}}{r}\right)+\frac{\eta}{r}\vec{\nabla}(\vec{r}\cdot\vec{v}). \tag{D11}$$

Here, the inner normal component is given by

$$\vec{\Pi}_n^<=\vec{\Pi}_n^<(\vec{r}=(\vec{R}_0+\zeta\vec{R}_0)^-) =\sum_{l,m}\left\{2\frac{\eta}{R_0^2}l(l-1)\varphi_{lm}^<+\frac{l^3-4l-3}{(l+1)(2l+3)}p_{lm}^<\right\}\mathrm{Y}_{lm}(x). \tag{D12}$$

The outer normal component reads

$$\vec{\Pi}_n^>=\vec{\Pi}_n^<(\vec{r}=(\vec{R}_0+\zeta\vec{R}_0)^+) =\sum_{l,m}\left\{2\frac{\eta}{R_0^2}(l+2)(l+1)\varphi_{lm}^>-\frac{l^3+3l^2-l}{l(2l-1)}p_{lm}^>\right\}\mathrm{Y}_{lm}(x). \tag{D13}$$

Finally, the difference between the inside and outside tangential component is given by

$$\vec{\Pi}_t^<-\vec{\Pi}_t^>=\sum_{l,m}\left\{2\frac{\eta}{R_0}[(l-1)\varphi_{lm}^<+(l+2)\varphi_{lm}^>] +\frac{l(l+2)}{(l+1)(2l+3)}p_{lm}^<-\frac{(l^2-1)}{l(2l-1)}p_{lm}^>\right\}\vec{\nabla}\mathrm{Y}_{lm}(x). \tag{D14}$$

[1] D.R. Nelson and B.I. Halperin, Phys. Rev. B **19**, 2457 (1979).
[2] J.M. Kosterlitz and D.J. Thouless, J. Phys. C **6**, 1181 (1973); A.P. Young, Phys. Rev. B **19**, 1855 (1979).
[3] L.D. Landau, Phys. Z. Sowjetunion **11**, 26 (1937).
[4] C.C. Grimes and G. Adams, Phys. Rev. Lett. **42**, 795 (1979).
[5] D.C. Glattli, E.Y. Andrei, and F.I.B. Williams, Phys. Rev. Lett. **60**, 420 (1998), and references therein.
[6] G. Deville, A. Valdes, E.Y. Andrei, and F.I.B. Williams, Phys. Rev. Lett. **53**, 588 (1984).
[7] D.S. Fisher, B.I. Halperin, and R. Morf, Phys. Rev. B **20**, 4692 (1979).
[8] R.H. Morf, Phys. Rev. Lett. **43**, 931 (1979).
[9] C.F. Chou, A.J. Jin, S.W. Hui, C.C. Huang, and J.T. Ho, Science **280**, 1424 (1998), and references therein.
[10] C. Knobler and R. Desai, Annu. Rev. Phys. Chem. **43**, 207 (1992).
[11] R. Seshadri and R.M. Westervelt, Phys. Rev. Lett. **66**, 2774 (1991).
[12] C.M. Murray, in *Bond Orientational Order in Condensed Matter Systems*, edited by K. Strandburg (Springer, Berlin, 1992).
[13] K. Zahn, R. Lenke, and G. Maret, Phys. Rev. Lett. **82**, 2721 (1999).
[14] A. Jaster, Phys. Rev. E **59**, 2594 (1999).
[15] K. Bagchi, H.C. Andersen, and W. Swope, Phys. Rev. E **53**, 3794 (1996).

[16] F.L. Somer, Jr., G.S. Canright, and T. Kaplan, Phys. Rev. E **58**, 5748 (1998).
[17] J. Park, T.C. Lubensky, and F.C. MacKintosh, Europhys. Lett. **20**, 279 (1992), and references therein.
[18] R.M.L. Evans, Phys. Rev. E **53**, 935 (1996).
[19] E.J. Davis, Aerosol. Sci. Technol. **26**, 212 (1997).
[20] P. Leiderer, Z. Phys. B: Condens. Matter **98**, 303 (1995).
[21] H.T. Chiang, V.S. Chen-White, R. Pindak, and M. Seul, J. Phys. II **5**, 835 (1995).
[22] C.C. Huang, in *Bond Orientational Order in Condensed Matter Systems*, edited by K. Strandburg (Springer, Berlin, 1992).
[23] F. Celestini, F. Ercolessi, and E. Tosatti, Phys. Rev. Lett. **78**, 3153 (1997).
[24] U. Albrecht and P. Leiderer, J. Low Temp. Phys. **86**, 131 (1992).
[25] P. Leiderer, in *Two-Dimensional Electron Systems*, edited by E.Y. Andrei (Kluwer Academic, Amsterdam, 1997).
[26] M.M. Salomaa and G.A. Williams, Phys. Rev. Lett. **47**, 1730 (1981).
[27] L.D. Landau, E.M. Lifshitz, and L.P. Pitaevskii, *Electrodynamics of Continuous Media*, 2nd ed. (Pergamon, New York, 1984).
[28] D.R. Nelson and L. Peliti, J. Phys. (France) **48**, 1085 (1987).
[29] P. Lenz and D.R. Nelson, Phys. Rev. Lett. **87**, 125703 (2001).
[30] U. Dierkes, S. Hildebrandt, A. Küster, and O. Wohlrab, *Minimal Surfaces I* (Springer, Berlin, 1992).
[31] D.R. Nelson, in *Phase Transitions and Critical Phenomena*, edited by C. Domb and J. Lebowitz (Academic, New York, 1983), Vol. 7.
[32] T. Frankel, *The Geometry of Physics* (Cambridge University Press, Cambridge, 1997).
[33] See, e.g., D.R. Nelson, Phys. Rev. B **28**, 5515 (1983); see also S. Sachdev and D.R. Nelson, J. Phys. C **17**, 5473 (1984).
[34] For the generalization to *p*-fold symmetric order parameters on the sphere see T. Lubensky and J. Prost, J. Phys. (France) **48**, 1085 (1987).
[35] M.J. Bowick, D.R. Nelson, and A. Travesset, Phys. Rev. B **62**, 8738 (2000).
[36] L.D. Landau and E.M. Lifshitz, *Hydrodynamics* (Pergamon, New York, 1959).
[37] Corrections to this spectrum arising from the nonlinear term of Eq. (13a) will be of higher order in r_{lm}. As can be seen from Eqs. (17), (18), and (25) $\rho_l(\vec{v}\cdot\vec{\nabla})\vec{v}$ is of order $R_0\omega^2 r_{lm}^2$, whereas the leading terms $\rho_l\partial\vec{v}/\partial t$ and $\vec{\nabla}p$ are of order $R_0\omega^2 r_{lm}$.
[38] D.R. Nelson and F. Spaepen, Solid State Phys. **42**, 1 (1989).
[39] S. Chandrasekhar, *Hydrodynamic and Hydromagnetic Stability* (Dover, New York, 1981).
[40] T.E. Faber, *Fluid Dynamics for Physicists* (Cambridge University Press, Cambridge, 1995).
[41] I.S. Gradshteyn and I.M. Rhyzik, *Table of Integrals, Series and Products*, 5th ed. (Academic Press, San Diego, 1994).
[42] Here, we have assumed as appropriate for helium, that the dielectric constants of the liquid and of its vapor phase are comparable $\varepsilon_l \simeq \varepsilon_v \simeq \varepsilon \simeq 1$. The general situation of a charged sphere with dielectric constant ε_1 in surrounding medium with dielectric constant ε_2 (with $\varepsilon_1 \neq \varepsilon_2$) is more complicated. However, in the limit of large N (when the radius of the sphere becomes large compared to interparticle spacing) one can in first order replace ε by $(\varepsilon_1+\varepsilon_2)/2$.
[43] V.B. Shikin, Pis'ma Zh. Eksp. Teor. Fiz. **27**, 44 (1978) [JETP Lett. **27**, 39 (1978)].
[44] For simplicity, the $l=0$ mode has been excluded here. However, bubbles are stabilized by their finite compressibility against purely radial oscillations.
[45] P. Lenz (unpublished).
[46] M.B. Schneider, J.T. Jenkins, and W.W. Webb, J. Phys. (France) **45**, 1457 (1984), and references therein.
[47] S.T. Milner and S.A. Safran, Phys. Rev. A **36**, 4371 (1987).
[48] The Reynolds number is $\mathrm{Re}=\rho v R_0/\eta$. A characteristic velocity is $v \simeq R_0/\tau$ with $\tau \simeq \eta R_0^3/\kappa$. Thus, $\mathrm{Re} \simeq \kappa\rho/\eta^2 R_0$. With κ of the order of $10\,k_BT$, $\eta/\rho \simeq 10^{-2}$ cm^2/sec, and $\rho \simeq 10^3$ kg/m^3 one has $\mathrm{Re} \simeq 10^{-5}$ for $R_0 \simeq 1$ μm. See also Ref. [47].
[49] U. Seifert, Eur. Phys. J. B **8**, 405 (1999).
[50] J. Happel and H. Brenner, *Low Reynolds Number Hydrodynamics* (Noordhoof, Leiden, 1973).
[51] M.A. Peterson, J. Math. Phys. **26**, 711 (1985).
[52] D.C. Morse and S.T. Milner, Phys. Rev. E **52**, 5918 (1995).
[53] In fact Milner and Safran find that r_{lm} diverges for $l=2$ in this case. Here, we do not take this instability into consideration. However, for a discussion of this point see also Ref. [54].
[54] U. Seifert, Adv. Phys. **46**, 13 (1997).
[55] F. David, E. Guitter, and L. Peliti, J. Phys. (France) **48**, 2059 (1987).
[56] R. Bar-Ziv and E. Moses, Phys. Rev. Lett. **73**, 1392 (1994).
[57] P. Nelson, T. Powers, and U. Seifert, Phys. Rev. Lett. **74**, 3384 (1995).
[58] Z. Zhang, H.T. Davis, and D.M. Kroll, Phys. Rev. E **48**, R651 (1993).
[59] S. Komura and R. Lipowsky, J. Phys. II **2**, 1563 (1992).
[60] S. Erdin and V.L. Pokrovsky, e-print cond-mat/0008266.
[61] F. David, in *Statistical Mechanics of Membranes and Interfaces*, edited by D. Nelson, T. Piran and S. Weinberg (World Scientific, Singapore, 1988).
[62] E. Kreyszig, *Differential Geometry* (Dover, New York, 1991).
[63] M. Nakahara, *Geometry, Topology and Physics* (IOP Publishing, London, 1990).